Submitted for publication in: *Journal of Non-Newtonian Fluid Mechanics*.

THE STABILITY OF VISCOELASTIC CREEPING PLANE SHEAR FLOWS WITH VISCOUS HEATING

L. E. BECKER† and G. H. MCKINLEY‡

†Courant Institute of Mathematical Sciences, New York University, New York, NY 10012-1185,
and
‡Department of Mechanical Engineering, Massachusetts Institute of Technology, Cambridge, MA 02139

December 21, 1999

Abstract − The two-dimensional linear stability of creeping plane Couette and Poiseuille flow of a viscoelastic fluid with viscous heating is investigated using a Galerkin-type Chebyshev collocation approach and a non-isothermal formulation of the FENE-P constitutive model. Viscous heating is observed to have a destabilizing/stabilizing tendency for Couette/Poiseuille flow at long to moderate disturbance wavelengths, and a stabilizing effect at short wavelengths, but no instabilities are found in the inertialess flow limit. Shear-thinning due to finite polymer extensibility reduces the base flow stresses as well as normal stress gradients at fixed Nahme number, and tends to further stabilize the flow, especially at short wavelengths. In addition to our non-isothermal results, our calculations indicate that creeping Poiseuille flow using the isothermal upper-convected Maxwell model is least-stable at high Deborah numbers to an odd mode with a wavenumber based on channel half-width of $k = 1.5$.

1 Introduction

Polymeric solutions and melts typically have zero-shear-rate viscosities that are three to eight orders of magnitude greater than the viscosity of water, and viscous heat generation is often important in industrial polymer processing applications (Pearson 1985). Heat conduction in polymeric materials is poor (thermal conductivity $k_c \sim 0.1\,\mathrm{W/m\,K}$), and hence frictional dissipation, even in the absence of externally applied heat sources, can cause significant temperature changes and gradients within a flowing polymeric fluid. These temperature increases in most cases do not appreciably alter the density ρ, the specific heat capacity C_p, or the thermal conductivity k_c, but do exponentially reduce the local viscosity and polymer elasticity. To date, viscous dissipation has usually been neglected in the study of Non-Newtonian fluid mechanics, even though thermally-induced gradients in viscosity and elasticity can significantly modify the corresponding isothermal flow and may possibly lead to new modes of elastic instabilities. In a series of papers, Shah and Pearson (1974abc) used a "Hele-Shaw"-style lubrication analysis to consider the stability of generalized Newtonian fluids incorporating viscous heating for pressure-driven flows in thin channels characteristic of injection molding geometries. Viscoelastic thermohydrodynamic instabilities have, however, received very little attention in the literature. Viscoelastic effects on Rayleigh-Benard convection have been reviewed by Petrie and Denn (1976) and by Larson (1992); the existence of a Hopf bifurcation and the resulting nonlinear dynamics of the over-stable oscillations predicted by the upper-convected Maxwell model have been analyzed by Khayat (1995), and experiments in heated micro-channels using DNA chains have been reported by Kolodner (1998). The effects of viscous heating on the stability of a viscoelastic flow without externally-imposed heating have not been considered.

In this paper, we examine the stability of Non-Newtonian plane Couette and Poiseuille flow with viscous heating, and the definition diagrams for these two flows are given in Figures 1(a) and 1(b), respectively.

[Figure 1 about here.]

The temperature dependence of the characteristic viscosity scale η_0 is taken to follow a Nahme-type law:

$$\eta_0 = \tilde{\eta}_0 e^{-\theta}, \tag{1}$$

where $\theta = \alpha(T - T_0)/T_0$ is a dimensionless temperature, and $\tilde{\eta}_0$ is the viscosity at the reference temperature T_0 . Typical values of the dimensionless heating coefficient α for polymeric solutions and melts range from 20 to 100 (Winter 1977). Less commonly used in the relevant literature on viscous heating is the Arrhenius-type law, in which the viscosity is taken to be proportional to $\exp\left[-\alpha(T - T_0)/T\right]$. Although this latter law is based more soundly on thermodynamics, and is able to fit data over a wider temperature range than the Nahme law, these two laws only differ appreciably for temperature differences larger than those commonly encountered in most viscous heating applications (Davis *et al.* 1983).

There are four dimensionless flow parameters governing this problem:

1. The Deborah number

$$De = \frac{\lambda_0 U_0}{h} \tag{2}$$

is the ratio of the characteristic relaxation time λ_0 of the polymer molecules, at the reference (wall) temperature T_0, to the convective time scale h/U_0.

2. The Nahme number
$$Na = \frac{\alpha\tilde{\eta}_0 U_0^2}{k_c T_0} \tag{3}$$
is a measure of the rate of heat generation by frictional dissipation relative to the rate of heat loss via conduction, and may be considered as the square of the ratio of a viscous heating time scale $\sqrt{\alpha\tilde{\eta}_0 h^2/(k_c T_0)}$ to the convective time scale h/U_0. Alternatively, we also define the Nahme number based on a characteristic stress instead of velocity, Na_τ, as
$$Na_\tau = \begin{cases} \dfrac{\alpha h^2 \tau^2}{\tilde{\eta}_0 k_c T_0} & \text{Couette} \\ \dfrac{\alpha h^4}{\tilde{\eta}_0 k_c T_0}\left(-\dfrac{dP}{dx}\right)^2 & \text{Poiseuille} \end{cases}, \tag{4}$$
where τ refers to the constant shear stress in Couette flow and dP/dx to the constant pressure gradient in Poiseuille flow. This latter dimensionless group Na_τ was denoted G in the early work by Gruntfest on the transient start-up of Couette flow with viscous heating (Gruntfest 1963). Plots of Na_τ versus Na represent the evolution of the dimensionless shear stress ($\propto \sqrt{Na_\tau}$) with increasing shear rate ($\propto \sqrt{Na}$) for a particular constitutive model and a chosen form of the temperature dependence of the material properties. For the Nahme heating model (1), such a plot shows a monotonic rise of Na_τ (or shear stress) with increasing Na (or shear rate) up to a single maximum or turning point, followed by a monotonic decay to zero. [The reader unfamiliar with the Nahme constitutive law may at this point wish to refer ahead to Figure 4(a), in which we present the constitutive relation between Na_τ and Na in Couette flow for the non-isothermal FENE-P model with different values of the polymer extensibility parameter b; the result for $b = \infty$ is equivalent to the analytic solution for Couette flow of a Newtonian fluid with viscous heating first obtained by Gavis and Laurence (1968).]

3. The Peclet number
$$Pe = \frac{\rho C_p U_0 h}{k_c} \tag{5}$$
is the ratio of the thermal diffusion time scale $\rho C_p h^2/k_c$ to the convective time scale h/U_0.

4. The Reynolds number
$$Re = \frac{\rho U_0 h}{\tilde{\eta}_0} \tag{6}$$
is the ratio of the viscous diffusion time scale $\rho h^2/\tilde{\eta}_0$ to the convective time scale h/U_0.

Due to the high viscosity and low thermal conductivity of polymeric solutions and melts, the Reynolds number is generally much less than one (the inertialess flow limit), the Peclet number is of the order of 10^3 to 10^6, and Deborah and Nahme numbers up to 50 might reasonably be expected in practical applications.

Under isothermal conditions, Newtonian (plane) Couette flow is linearly stable at all Reynolds numbers, and Newtonian (plane) Poiseuille flow is linearly stable below a critical Reynolds number of $Re_c = 5772.22$ (Drazin and Reid 1982, Orszag 1971). Isothermal viscoelastic Couette flow is linearly stable for the (upper-convected) Maxwell constitutive model (Renardy and Renardy 1986, Gorodtsov and Leonov 1967) as well as for the Oldroyd-B model (Wilson *et al.* 1998). Analyses with the second-order fluid and UCM/Oldroyd-B constitutive models show that elasticity destabilizes isothermal plane Poiseuille flow to infinitesimal disturbances, and critical Reynolds numbers down to $Re_c \leq 2000$ have been computed (Sureshkumar and Beris 1995, Lee and Finlayson 1986, Porteus and Denn 1972). Sureshkumar and Beris (1995) also demonstrated the stabilizing effect on Poiseuille flow of finite polymer extensibility for the (constant viscosity) Chilcott-Rallison model, which reduces to the Oldroyd-B model in the limit of infinite extensibility. At low Reynolds numbers of order one or less, both isothermal plane Couette and Poiseuille flows appear to be stable, except for the case of co-extruded liquids in channel flows with jumps in viscosity and/or normal stresses across the fluid-fluid interface (*e.g.* Wilson and Rallison 1997, Su and Khomami 1992).

Recently, Wilson and Rallison (1999) considered the stability of planar channel flows with a continuous stratification in material properties across the channel. Calculations showed that the flow can be destabilized for sufficiently steep cross-stream gradients in the fluid elasticity or other material properties. Given the poor thermal conductivity of polymeric fluids ($Pe \gg 1$) and the high shear rates near the wall, steep gradations in the viscoelastic material properties may be expected during processes such as injection molding, and it has been conjectured that instabilities such as "stick-slip" may be caused or modified by viscous heating effects (Hatzikiriakos *et al.* 1997).

Choosing the Nahme law for the viscosity in the Newtonian constitutive relation, Sukanek *et al.* (1973) used a Galerkin technique with only four terms in each approximation series to determine that plane Couette flow with viscous heating is linearly stable at low Reynolds numbers and that it can become unstable for moderate Reynolds and Nahme numbers. Ho *et al.* (1977), employing a shooting technique, found these results to be quantitatively in error, but still concluded that both plane Couette and Poiseuille flows with viscous heating (without elastic effects) are stable at low Reynolds numbers. Yueh and Weng (1996), apparently unaware of the work by Ho *et al.*, thoroughly recalculated the work of Sukanek *et al.* for both Nahme- and Arrhenius-type laws using a more accurate Chebyshev spectral approach. Their results again show a significant quantitative disagreement with those of Sukanek *et al.*, but also indicate instabilities only for moderate to high Reynolds and Nahme numbers. For more general viscosity versus temperature dependences, Joseph (1964, 1965) presented some base flow results and showed that inviscid Couette flow is linearly unstable on that branch of the constitutive curve where the stress is a decreasing function of shear rate (the "upper" branch), a result which is loosely confirmed by Yueh and Weng (1996) for the Arrhenius law in the inviscid limit only. Johns and Narayanan (1997) performed a zero-wavenumber perturbation analysis for frictional heating in plane Couette flow, and determined that the only point of neutral stability occurs at the "nose" of the constitutive curve (where the shear stress is a maximum) when wall stress, as opposed to wall speed, acts as the control variable. The result that the nose is a point of neutral stability to zero-wavenumber perturbations at constant stress appears reasonable, since no steady (uni-directional) base flow exists for stresses greater than

at the nose. We do not, however, share their opinion that their basic result by itself suggests the upper branch of the constitutive curve is unstable, which, at least for low Reynolds numbers, would contradict all of the more rigorous stability analyses cited above.

The combined effects of viscous heating and polymer elasticity upon the stability of plane shear flows have never been investigated, and in this work we examine the linear stability of creeping plane Couette and Poiseuille flows with Nahme-type viscous heating for a non-isothermal form of the FENE-P constitutive model.

2 Formulation

2.1 Governing Equations

In addition to the continuity equation for incompressible flow,

$$\nabla \cdot \boldsymbol{u} = \boldsymbol{0}, \tag{7}$$

and the Cauchy momentum equation,

$$Re\frac{D\boldsymbol{u}}{Dt} = \nabla \cdot \boldsymbol{\pi}, \tag{8}$$

where $\boldsymbol{\pi}$ is the non-dimensionalized total stress tensor, a viscous heating formulation must also take into account the energy equation

$$Pe\frac{D\theta}{Dt} = \nabla^2\theta + Na\,\boldsymbol{\pi} : \nabla\boldsymbol{u}. \tag{9}$$

These equations have been non-dimensionalized with a characteristic length scale h, velocity scale U_0, time scale h/U_0, and stress scale $\tilde{\eta}_0 U_0/h$.

For our constitutive relation, we chose a non-isothermal form of the standard isothermal FENE-P dilute-solution dumbbell model (Bird *et al.* 1987b). Assuming that temperature gradients on the scale of a polymer molecule are negligible so that the isothermal model applies locally, we define a characteristic polymeric viscosity $\eta_p = (nk_BT)\lambda(T)$ and let $\eta_0 = \eta_s + \eta_p$, where n is the number of dumbbells per unit volume, k_B is the Boltzmann constant, and η_s is the solvent viscosity. Each of these viscosities is assumed to follow the Nahme law of Equation (1) with the same dimensionless heating coefficient α, and hence the characteristic relaxation time of the polymer molecules at temperature T, $\lambda(T)$, varies with $\lambda(T_0) = \lambda_0$ as

$$\lambda(T) = \lambda_0 \left(\frac{T_0}{T}\right) e^{-\theta} = \frac{\lambda_0 e^{-\theta}}{1 + \theta/\alpha}\,. \tag{10}$$

The justification and internal consistency of such a molecular approach has been discussed by Marrucci (1972). Alternative non-isothermal formulations involving differential constitutive equations have recently been developed by Peters and Baaijens (1997).

The non-dimensionalized total stress tensor $\boldsymbol{\pi}$ is then given by

$$\boldsymbol{\pi} = -p\boldsymbol{\delta} + \beta e^{-\theta}\left[\nabla\boldsymbol{u} + (\nabla\boldsymbol{u})^T\right] + \left(\frac{1-\beta}{De}\right)\left(\frac{T}{T_0}\right)\left[f(tr(\boldsymbol{A}))\boldsymbol{A} - \left(\frac{b}{b+2}\right)\boldsymbol{\delta}\right], \tag{11}$$

where p is the pressure, $\boldsymbol{\delta}$ the unit tensor, β the solvent viscosity ratio η_s/η_0, $\boldsymbol{A}$ the momentum- and phase-space-averaged dumbbell configuration tensor, b the dimensionless square of the dumbbell end-to-end length, and the function f follows the Warner force law

$$f(tr(\boldsymbol{A})) = \frac{1}{1 - tr(\boldsymbol{A})/b} \tag{12}$$

(see Bird *et al.* 1987b). The configuration tensor $\boldsymbol{A}$ evolves according to the convection-diffusion equation

$$De \left(\frac{T_0}{T}\right) e^{-\theta} \boldsymbol{A}_{(1)} + f(tr(\boldsymbol{A}))\boldsymbol{A} - \left(\frac{b}{b+2}\right)\boldsymbol{\delta} = \boldsymbol{0}, \tag{13}$$

where $\boldsymbol{A}_{(1)}$ denotes the upper-convected derivative of $\boldsymbol{A}$,

$$\boldsymbol{A}_{(1)} = \frac{\partial \boldsymbol{A}}{\partial t} + \boldsymbol{u} \cdot \nabla \boldsymbol{A} - \boldsymbol{A} \cdot \nabla \boldsymbol{u} - (\nabla \boldsymbol{u})^T \cdot \boldsymbol{A}\,. \tag{14}$$

The two scalar equations of continuity and energy, the vector equation of momentum conservation, together with the tensor diffusion equation for dumbbell configuration, form a consistent set for the determination of the unknowns $\boldsymbol{u}$, p, θ, and $\boldsymbol{A}$. The transient stress growth for such a model following the inception of steady shear flow under adiabatic conditions has been considered by Wiest (1996).

2.2 Solution Procedure

For the steady, uni-directional Couette and Poiseuille base flows depicted in Figures 1(a) and 1(b), respectively, the above set of governing equations is solved iteratively using the IMSL subroutine DMOLCH, except for the cases of Oldroyd-B (polymer extensibility $b \to \infty$) and Newtonian Couette flow. In the latter case, the exact analytical solution was derived by Gavis and Laurence (1968):

$$U(y) = \frac{1}{2}\left\{1 + \sqrt{\frac{8+Na}{Na}}\,\tanh\left[\left(\operatorname{arcsinh}\sqrt{Na/8}\right)(2y-1)\right]\right\}, \tag{15}$$

$$\Theta(y) = \ln\left\{(1+Na/8)\,\operatorname{sech}^2\left[\left(\operatorname{arcsinh}\sqrt{Na/8}\right)(2y-1)\right]\right\}. \tag{16}$$

An equivalent result is obtained for the Oldroyd-B model, with the addition of a non-zero normal stress (treated later in Equation 24) which does not contribute to the dissipation term in the energy equation (9). Base flow profiles along with constitutive plots for Couette and Poiseuille flows are presented in the following section.

For the linear stability analysis, we consider only two-dimensional disturbances in the (x, y) plane, which are uniform in the z-direction. The three-dimensional linear stability problem for isothermal plane shear flows can in many cases be reduced to a two-dimensional one which is more stable than that for purely two-dimensional perturbations. This transformation is known as Squire's theorem (Drazin and Reid 1982), but as noted by Sukanek *et al.* (1973), such a transformation does not appear possible for the viscous heating problem. Given the complexity of the present analysis,

we restrict ourselves here to two-dimensional disturbances and leave the three-dimensional stability analysis for future work.

The complete set of governing equations presented in the previous subsection is linearized for infinitesimal two-dimensional perturbations about the base flow using the symbolic manipulation program Maple. These stability equations are subsequently reduced, by the usual elimination of continuity and pressure, to six non-trivial partial differential equations for the six unknown disturbance variables $(v, \theta, a_{xx}, a_{xy}, a_{yy}, a_{zz})$, where v is the cross-stream component of velocity, θ now refers specifically to the perturbation in temperature, and the four non-zero a_{ij} refer to the perturbations in the dumbbell configuration tensor $\boldsymbol{A}$. It does not appear possible (or insightful) to represent this set of equations in a compact format suitable for publication due to the enormous numbers of terms involved; interested readers may obtain the Maple script from the authors upon request.

We seek to examine the growth of modes proportional to $\exp[ikx+\sigma t]$, where k is the wavenumber and σ is the complex eigenvalue. Unstable modes correspond to those with $\mathrm{Re}(\sigma) > 0$. As has become customary in linear stability analyses since the work of Orszag (1971) on the Orr-Sommerfeld equation, we use Chebyshev polynomials to best approximate variations in the cross-stream (y) direction (Fornberg 1995 gives an excellent recent treatise on pseudospectral methods). In particular, we consider Galerkin-type expansions of shifted Chebyshev polynomials $T_r^*(y)$ for the disturbance velocity component v and the disturbance temperature θ of the form:

$$v(x,y,t) = \mathrm{Re}\left\{\left[\sum_{r=0}^{N} a_r\left[y^4+\chi_1 y^3+\chi_2 y^2+\chi_3 y+\chi_4\right]T_r^*(y)\right]\exp[ikx+\sigma t]\right\} \tag{17}$$

$$\theta(x,y,t) = \mathrm{Re}\left\{\left[\sum_{r=0}^{N} b_r\left[y^2+\chi_5 y+\chi_6\right]T_r^*(y)\right]\exp[ikx+\sigma t]\right\} . \tag{18}$$

The parameter vector $\boldsymbol{\chi} = (\chi_1, \chi_2, \chi_3, \chi_4, \chi_5, \chi_6)^T$ is in general a function of the index r and is chosen here so that each term of the expansion for v and the expansion for θ satisfies individually the no-slip boundary condition ($v = 0$ and $\partial v/\partial y = -\partial u/\partial x = 0$) and the constant wall temperature boundary condition ($\theta = 0$), respectively, on both the top ($y = 1$ Couette, $y = 2$ Poiseuille) and bottom ($y = 0$) walls. In our case, these conditions correspond to $\boldsymbol{\chi} = (-2, 1, 0, 0, -1, 0)^T$ for Couette flow and $\boldsymbol{\chi} = (-4, 4, 0, 0, -2, 0)^T$ for Poiseuille flow. Our choice of Galerkin-type expansions satisfying boundary conditions is particularly simple and convenient for our subsequent collocation procedure to construct a generalized eigenvalue problem, and for our numerical analysis performs no better or worse than previously reported Galerkin expansions of the same order such as those obtained by the method of integrating the highest derivative (Zebib 1987). The four disturbance configuration functions a_{ij} are not required to satisfy further boundary conditions, and are expanded as regular series of shifted Chebyshev polynomials:

$$a_{xx}(x,y,t) = \mathrm{Re}\left\{\left[\sum_{r=0}^{N} c_r T_r^*(y)\right]\exp[ikx+\sigma t]\right\} , \tag{19}$$

$$a_{xy}(x,y,t) = \mathrm{Re}\left\{\left[\sum_{r=0}^{N} d_r T_r^*(y)\right]\exp[ikx+\sigma t]\right\} , \tag{20}$$

$$a_{yy}(x,y,t) = \mathrm{Re}\left\{\left[\sum_{r=0}^{N} e_r T_r^*(y)\right]\exp[ikx+\sigma t]\right\}, \quad (21)$$

$$a_{zz}(x,y,t) = \mathrm{Re}\left\{\left[\sum_{r=0}^{N} f_r T_r^*(y)\right]\exp[ikx+\sigma t]\right\}. \quad (22)$$

A generalized complex eigenvalue problem

$$\boldsymbol{M}\boldsymbol{x} = \sigma \boldsymbol{N}\boldsymbol{x} \quad (23)$$

with $6(N+1)\times 6(N+1)$ coefficient matrices $\boldsymbol{M}$ and $\boldsymbol{N}$ for the eigenvector of complex expansion coefficients, $\boldsymbol{x}$, is generated by substituting the above expansions into the linearly perturbed set of six governing equations and collocating at the $(N+1)$ roots of $T_{N+1}^*(y)$ in order to minimize the maximum spectral approximation error over the domain (Fornberg 1995). This collocation procedure yields the same order of accuracy as the more common application of orthogonality, which, as pointed out by Zebib (1987), can remove the two large, positive, but spurious eigenvalues found by Orszag (1971) for the Orr-Sommerfeld equation using the Lanczos-tau method. In our collocation formulation, we still obtain these two spurious modes at non-zero Reynolds numbers, the eigenvalues of which increase in magnitude with increased spectral resolution. At zero Reynolds number, there are no spurious modes at all except when the solvent viscosity is identically zero (corresponding to the upper-convected Maxwell constitutive model), and this limit may be conveniently investigated by retaining a small but finite amount of solvent viscosity, say $\beta = 10^{-4}$. The work of Graham (1998) suggests that these spurious modes are a result of eliminating pressure in such stability calculations, and that it is further possible to eliminate spurious modes by imposing numerical Neumann conditions on stresses at the boundary collocation points; we did not investigate such issues in this work. The generalized eigenvalue problem of Equation (23) was solved using the IMSL routine DGVCCG.

3 Base Flow Results

3.1 Couette Flow

The exact analytical solution for Couette flow with viscous heating presented in Equations (15) and (16) applies in the limit of infinite polymer extensibility ($b \to \infty$), and is depicted graphically in Figures 2 and 3 for $Na = 0$, 10, and 100.

[Figure 2 about here.]

[Figure 3 about here.]

As the Nahme number increases with increasing shear rate, the steady-state temperature rises monotonically due to frictional dissipation and is maximum at the center of the channel, the bounding walls of which are maintained at the constant reference temperature T_0. The viscosity becomes correspondingly lower in the channel, so that more and more of the fluid above mid-plane

(less below) is dragged along with the top plate than in the isothermal case ($Na = 0$) with a linear velocity profile. Further description of this base flow is given in the original paper by Gavis and Laurence (1968).

Next we turn our attention to the effect of finite polymer extensibility, and also highlight in Figures 2 and 3 the differences in the non-dimensionalized velocity and temperature profiles arising when the finite extensibility parameter is decreased from $b = \infty$ to $b = 10$ for the case of $Na = 10$, $De = 10$, $\alpha = 60$, and $\beta = 0.5$. We chose $De = 10$ to show strong elastic effects, $\alpha = 60$ to match polystyrene, and $\beta = 0.5$ to model common Boger fluids which contain significant amounts of viscous solvent. Finite extensibility is responsible for shear-thinning of the polymeric contribution to the total viscosity as well as for a reduction in elastic stresses (see Bird *et al.* 1987b for a detailed discussion), and hence for the same Nahme number, the velocity and temperature profiles for $b = 10$ are less influenced by viscous heating than those for infinite extensibility.

Both viscous heating and finite extensibility tend to reduce the normal stress τ_{xx} ($\boldsymbol{\tau} = \boldsymbol{\pi} + p\boldsymbol{\delta}$), which, for Couette flow, is nearly constant over the entire channel. Using the Oldroyd-B model ($b = \infty$), the formula relating the non-dimensionalized normal and shear stress components is particularly simple:

$$\tau_{xx} = \frac{2(1-\beta)De\,\tau_{xy}^2}{1+\theta/\alpha}. \tag{24}$$

Since the shear stress is constant for Couette flow (an immediate consequence of conservation of x-momentum), the variations in normal stress across the gap are small and result from the weak dependence on temperature through the factor $(1 + \theta/\alpha) = (T/T_0)$. For Poiseuille flow on the other hand, the topic of the following subsection, the shear stress varies linearly across the channel, resulting in quadratic variations in normal stress. Varying the dimensionless heating coefficient α, in the range $\alpha \in [20, 100]$, by itself does not appreciably affect any of our results if the Nahme number is kept unchanged; a large value of α is, however, essential for achieving Nahme numbers greater than one in most practical applications.

Base flow constitutive plots for Couette flow of Na_τ versus Na (dimensionless square of shear stress versus that of shear rate) and of normal stress at the wall versus Na are presented in Figures 4(a) and (b), respectively, where $De = 10$, $\alpha = 60$, $\beta = 0.5$, and $b = 10$, 1000, and ∞.

[Figure 4 about here.]

The wall shear stress reaches a maximum near $Na = 18.2$ for $b = \infty$, and the plots again show that finite polymer extensibility significantly lowers both the shear and normal stresses at fixed Nahme and Deborah number. It is important to note that viscous heating dominates viscoelastic effects at high Nahme numbers, and in each plot the curves for finite values of b approach those for infinite extensibility as $Na \to \infty$. The monotonic trends of the base flow profiles with increasing Nahme number, as shown in Figures 2 and 3, continue unaffected by the maximum in Na_τ, and the same holds true for the stability results treated later; at low Reynolds numbers, there are no qualitative changes associated with increasing the Nahme number beyond the local turning point in the shear stress.

3.2 Poiseuille Flow

No analytical solutions exist for Poiseuille flow with viscous heating, and Figures 5 and 6 respectively show our numerically computed velocity and temperature profiles in the limit of infinite extensibility for $Na = 0$, 10, and 100.

[Figure 5 about here.]

[Figure 6 about here.]

The steady-state temperature again increases monotonically with Nahme number, and is maximum at the center of the channel ($y/h = 1$) even though the shear rate (and hence frictional dissipation) is zero there. The majority of the heat is viscously generated close to the stationary walls, from where it conducts both outward into the constant-temperature boundaries as well as inward. The decreased viscosity in the interior of the channel results in enhanced convective transport of fluid elements near the mid-plane ($y/h = 1$) relative to those near the bounding walls.

We also indicate in Figures 5 and 6 the effect of finite polymer extensibility upon the velocity and temperature fields in plane Poiseuille flow by considering the case of $b = 10$ with $Na = 10$, $De = 10$, $\alpha = 60$, and $\beta = 0.5$. As observed for Couette flow, the additional shear-thinning due to finite extensibility results in velocity and temperature profiles which, for the same Nahme number, are less influenced by viscous heating than those for infinite extensibility. The variation in the normal stress τ_{xx} across the channel is shown in Figure 7. Note that the pressure varies linearly along the channel, but not across the channel. Thus the normal stress $\tau_{yy} \equiv 0$, and τ_{xx} also represents the first normal stress difference.

[Figure 7 about here.]

In sharp contrast to plane Couette flow, the normal stress varies significantly across the channel and is maximum at the walls ($y/h = 0, 2$). As the FENE parameter b is decreased at fixed values of De and Na, this continuous stratification in the elasticity of the fluid is reduced both in magnitude and in its rate of variation.

Constitutive plots for the Poiseuille base flow are presented in Figure 8 for constant $De = 10$, $\alpha = 60$, and $\beta = 0.5$, with $b = 10$, 1000, and ∞. In Figure 8(a) we show the variation of Na_τ, a dimensionless square of the pressure gradient, versus Na, a dimensionless square of the flow rate. The wall shear stress reaches a maximum near $Na = 8.2$ for $b \to \infty$, and pressure-driven flows are unstable beyond this turning point in the pressure gradient. Recent experiments with Newtonian fluids (Skul'skiy *et al.* 1999) have demonstrated that beyond this point the flow "jumps" to a new supercritical state which cannot be captured by the Nahme law, but which can be described using the more realistic Arrhenius form of the thermal dependence of the viscosity (Davis *et al.* 1983).

[Figure 8 about here.]

The variation in the (maximum) normal stress at the wall is given in Figure 8(b). The calculations again show that finite polymer extensibility significantly lowers the magnitude of the normal stresses at fixed Nahme and Deborah numbers. In addition, the effects of polymer extensibility become less and less important as viscous heating increasingly dominates at large Nahme numbers.

4 Stability Results

In this section, we present results for the linear stability of viscoelastic plane Couette and Poiseuille flows with viscous heating at zero Reynolds number ($Re = 0$).

4.1 Couette Flow

We begin with an examination of the eigenvalue spectrum. Figure 9(a) gives the spectrum at a wavenumber of $k = 1$ for the case of $Pe = 10^4$, $Na = 0$, $De = 10$, $\alpha = 60$, $\beta = 0.5$, and $b = \infty$, as computed with $N = 250$ terms in each spectral approximation series.

[Figure 9 about here.]

Since the Nahme number is identically zero here, the energy disturbance equation decouples from the continuity and momentum equations, and reduces to:

$$\frac{d^2\theta}{dy^2} = \left[(ikPe)y + \sigma Pe + k^2\right]\theta. \tag{25}$$

This equation may be transformed into the standard Airy equation, from which the (energy) eigenvalues σ, subject to the constant-temperature boundary conditions ($\theta = 0$ at $y = 0$, 1), may be determined as solutions to the equation

$$Ai(s_0)Bi(s_1) = Ai(s_1)Bi(s_0), \tag{26}$$

where Ai and Bi are the two linearly independent Airy functions, $s_0 = -(\sigma Pe + k^2)/(kPe)^{2/3}$, and $s_1 = -(ikPe + \sigma Pe + k^2)/(kPe)^{2/3}$.

The zero-Nahme-number spectrum of Figure 9(a) is composed of these energy eigenvalues (represented by hollow circles) and of those from the isothermal flow problem (solid circles). The two least-stable isothermal modes in our case of $\beta = 0.5$ are analogous to the two discrete modes for the Maxwell model ($\beta = 0$) found analytically by Gorodtsov and Leonov (1967), and the remaining discrete modes are due to the presence of the viscous solvent. The two continuous line spectra, spanning the complete range of possible values of $\mathrm{Im}(\sigma)$, correspond to the isothermal non-analytic modes, which are located at $\sigma = -1/De - iky_s$ and at $\sigma = -1/(\beta De) - iky_s$ with $y_s \in [0, 1]$. The former continuous spectrum is difficult to resolve, and appears as a balloon which converges to a line with increasing spectral resolution; the corresponding eigenmodes have a discontinuity in $v'''(y)$ along with singular stresses (and a_{ij}) at a position $y = y_s$ in the channel. A more detailed discussion of the continuous spectrum is presented in the appendix by Graham (1998) and in Wilson *et al.* (1998). Note that the overall least-stable eigenvalue in Figure 9(a) ($k = 1$) corresponds to an energy eigenmode. At higher wavenumbers, the situation changes as the energy modes become increasingly stable, while the temporal parts of the eigenvalues, $\mathrm{Re}(\sigma)$, for the viscoelastic modes increase monotonically and asymptotically approach a constant value. In the limit of large Deborah number and wavenumber, the (two) least-stable isothermal Maxwell modes are known to obey $\mathrm{Re}(\sigma) = -1/(2De)$.

The spectrum for $k = 1$, under conditions identical to those in Figure 9(a) but with a Nahme number of five instead of zero, is shown in Figure 9(b). Although the energy and isothermal viscoelastic modes are now coupled, it turns out that the (two) least-stable modes are very similar to the corresponding original energy modes, and that they become increasingly stable at higher wavenumbers. Hence we shall still refer to them as energy modes, and as will be shown shortly, modes which are predominantly viscoelastic in character dominate at high wavenumber in a manner akin to the case of zero Nahme number described above.

Next we briefly discuss the convergence of our spectral approximation for the discrete, analytic eigenmodes. Figure 10 shows the convergence with increasing number of terms r of the coefficient c_r, from the spectral approximation series of a_{xx} given in Equation (19), for the least-stable eigenvalues at wavenumbers $k = 1$ and $k = 5$, where $Pe = 10^4$, $Na = 5$, $De = 10$, $\alpha = 60$, $\beta = 0.5$, and $b = \infty$.

[Figure 10 about here.]

While the $k = 1$ mode is an energy mode and the $k = 5$ a viscoelastic mode, it appears generally true that convergence in the presence of viscoelasticity becomes increasingly slow with increasing wavenumber, apparently due to localized regions of relatively large polymeric stresses that develop as the secondary flow vortices move closer to either wall with increasing wavenumber. As discussed in connection with the base flow solutions, both viscous heating and finite extensibility tend to reduce elastic stresses, and it is indeed observed that either of these two effects can allow for convergence in cases of high Deborah number and wavenumber for which no convergence may otherwise be obtained (to $N = 300$) under isothermal conditions and/or infinite extensibility.

Our overall results are summarized in Figures 11 to 15, in which we plot the temporal part of the least-stable eigenvalue, $\mathrm{Re}(\sigma_{max})$, versus wavenumber k for a range of conditions at zero Reynolds number with $\alpha = 60$.

[Figure 11 about here.]

In particular, Figure 11 shows the exact agreement of our results at zero Nahme number ($Pe = 10^4$, $De = 5$, $b = \infty$) for $\beta = 0$ (solid circles) with the energy eigenvalues of Equation (25) at low to moderate wavenumbers and with those of the isothermal Maxwell problem at higher wavenumbers. There is a sharp cross-over in the curve for $\mathrm{Re}(\sigma_{max})$ at the point where the viscoelastic modes overtake the energy modes as least-stable in the spectrum at higher wavenumbers. This cross-over point is slightly delayed for the case of $\beta = 0.5$ (hollow circles), due to the stabilizing effect of the viscous solvent on the isothermal viscoelastic modes. The curve for $Na = 5$ and $\beta = 0$ (solid line) indicates both the destabilizing effect of viscous heating at moderate wavenumber and the stabilizing effect relative to the isothermal Maxwell modes at high wavenumber. We could not obtain convergence beyond a wavenumber of $k \approx 8$ for the isothermal viscoelastic modes at a Deborah number $De = 5$ with up to $N = 300$ terms in each expansion, and slightly less so for the case of $\beta = 0.5$ relative to that of $\beta = 0$ as the discrete modes are closer to and engulfed sooner by the expanding balloon of the poorly resolved continuous spectrum (see Wilson *et al.* 1998 for spectra with larger balloons). The presence of viscous heating, however, reduces the elastic stresses and speeds their convergence, so that for $Na = 5$ we are able to obtain converged solutions to just beyond $k = 10$.

The destabilizing effect of viscous heating at moderate wavenumbers is demonstrated in Figure 12 for $Na = 5$, 10, and 50 with $Pe = 10^4$, $De = 5$, $\beta = 0.5$, and $b = \infty$.

[Figure 12 about here.]

We did not investigate Nahme numbers greater than 100, as such high Nahme numbers are not encountered in practical applications. The viscoelastic modes are increasingly stable with increasing Nahme number, so that the above-mentioned cross-over point in the curve occurs at higher and higher wavenumbers. The consequences of changes in Peclet number are illustrated in Figure 13 for $Pe = 10^3$, 10^4, and 10^5 at a Deborah number of $De = 10$.

[Figure 13 about here.]

Increasing the Peclet number also causes a destabilization of the energy modes at moderate wavenumber, but, unlike the case of increasing Nahme number, does not significantly affect the viscoelastic modes at high wavenumber. The stabilizing effect of increased solvent proportions on the viscoelastic modes is shown in Figure 14, and that of finite extensibility in Figure 15.

[Figure 14 about here.]

[Figure 15 about here.]

Increasing the solvent viscosity ratio β and/or decreasing the extensibility parameter b has a slight stabilizing effect on the energy modes, and a more significant one on the viscoelastic modes.

Before concluding our presentation of results for inertialess viscoelastic plane Couette flow, we consider two sets of streamline and contour plots for one of each pair of least-stable eigenvalues at wavenumbers $k = 1$ and $k = 5$, respectively, where $Pe = 10^4$, $Na = 5$, $De = 10$, $\alpha = 60$, $\beta = 0.5$, and $b = \infty$. In the first set at a wavenumber of $k = 1$, we examine the (energy) eigenmode for the eigenvalue $\sigma = -0.043 - 0.992i$, which is the larger in magnitude of the least-stable pair. This eigenmode has a (dimensionless) wave speed of 0.992 and travels with the top wall, while the other mode of the pair is nearly stationary with a wave speed of 0.078. The streamlines of both modes look identical, except that the faster moving mode is composed of vortices closer to the top wall while the slower moving one consists of a similar array of vortices closer to the lower wall. The perturbation streamlines for the faster of the least-stable eigenvalues at $k = 1$ are given in Figure 16, indicating regions of extensional flow near the walls where the streamlines diverge.

[Figure 16 about here.]

The corresponding contour plots of the xx-component of the disturbance configuration tensor $\boldsymbol{a}$ and of the disturbance temperature θ are presented in Figures 17 and 18, respectively, showing a strong variation only near the top wall.

[Figure 17 about here.]

[Figure 18 about here.]

The disturbance configuration function a_{xx}, which for $b = \infty$ is proportional to the stress τ_{xx}, is in general larger in magnitude than the other components of $\boldsymbol{a}$ and slowest to converge. Relatively large positive values of a_{xx} and θ apparently develop near the upper wall where the perturbation flow opposes the motion of the upper wall, creating regions of increased shear.

These results with $k = 1$ may be compared to those with $k = 5$ for the (viscoelastic) eigenmode of $\sigma = -0.074 - 0.067i$, the smaller of the least-stable pair; the perturbation streamlines for this latter mode are shown in Figure 19.

[Figure 19 about here.]

This eigenmode is nearly stationary with a wave speed of 0.013, and has an array of vortices closer to the bottom wall. As the wavenumber increases, the vortices in general move closer and closer to the top and bottom walls, causing large variations of all perturbation quantities in the region between the vortex and the wall. This variation is largest for a_{xx}, and, in the narrowing boundary layer, is qualitatively similar to that for $k = 1$ (Figs. 17 and 18); values over the rest of the channel are negligible in comparison. The eigenfunctions at high wavenumber hence contain large spikes near either the top or the bottom wall which become increasingly difficult to resolve, as observed by Sureshkumar and Beris (1995).

4.2 Poiseuille Flow

We again begin with an examination of the eigenvalue spectrum. Figure 20(a) gives the spectrum at a wavenumber of $k = 1.5$ for the case of $Pe = 10^3$, $Na = 0$, $De = 5$, $\alpha = 60$, $\beta = 0.5$, and $b = \infty$, as computed with $N = 250$ terms in each spectral approximation series.

[Figure 20 about here.]

At zero Nahme number, the energy modes (hollow circles) at this wavenumber dominate the isothermal viscoelastic modes (solid circles), and there no longer exist the pairs of discrete eigenvalues with the same temporal part as were observed for Couette flow. No analytical solutions are known for the stability of Poiseuille flow. When the Nahme number is increased to $Na = 20$, as shown in Figure 20(b), the spectrum is further dominated by energy modes, due to the reduction in polymeric stresses caused by viscous heating. The discussion of convergence for Couette flow applies equally well to Poiseuille flow, except that convergence of the viscoelastic modes is even more difficult to achieve for the same Deborah number and wavenumber.

Our results for Poiseuille flow are summarized in Figures 21 and 22, in which we plot the temporal part of the least-stable eigenvalue, $\mathrm{Re}(\sigma_{max})$, versus wavenumber k for a range of conditions at zero Reynolds number with $\alpha = 60$.

[Figure 21 about here.]

Figure 21 shows the effect of increasing Nahme number at $Pe = 10^3$, $De = 5$, $\beta = 0.5$, and $b = \infty$. In contrast to our findings for Couette flow, viscous heating tends to stabilize at all wavenumbers. The energy modes again dominate at low to moderate wavenumbers, while viscoelastic modes dominate at high wavenumbers. The cross-over point of the $Na = 0$ curve is not shown, as convergence could

not be obtained (to $N = 300$) for the viscoelastic modes at that range of wavenumbers. We also present our computations for the isothermal Maxwell model ($\beta = 0$), the curve for which shows a maximum near $k = 1.5$ and terminates where convergence is lost. By symmetry, each mode is either even (sinuous) or odd (varicose) in the cross-stream component of the disturbance velocity, v, about the mid-plane of the channel. The least-stable energy modes shown in Figure 21 are always odd, and the least-stable viscoelastic modes after the cross-over point appear to be always even (at least until loss of convergence). The least-stable modes for the isothermal Maxwell model are odd below a wavenumber of about $k = 3$ and even above.

Figure 22 presents our results obtained with a higher Peclet number of $Pe = 10^4$ at a Deborah number of $De = 10$.

[Figure 22 about here.]

Increasing Peclet number, as observed for Couette flow, destabilizes the flow at moderate wavenumber, but viscous heating, specified by the Nahme number, is still stabilizing at all wavenumbers. No cross-over points fall within the domain of this plot; the curve for $Na = 0$ is terminated at the point where unresolved viscoelastic modes dominate. The maximum in the curve for the isothermal Maxwell model is again near $k = 1.5$, and all modes for points shown in the figure are odd. Unconverged results again suggest that the least-stable isothermal Maxwell modes above about $k = 3$ are even.

Perturbation streamlines are presented in Figure 23 for the eigenmode of the least-stable eigenvalue, $\sigma = -0.061 - 2.95i$, at a wavenumber of $k = 3$ with $Pe = 10^3$, $Na = 20$, $De = 5$, $\alpha = 60$, $\beta = 0.5$, and $b = \infty$.

[Figure 23 about here.]

This odd or varicose energy mode, depicted over the lower half-channel region $0 \leq y \leq 1$, travels close to the centerline velocity at a wave speed of 0.983, and consists of an array of cells containing two vortices each. For the least-stable mode, the vortices closer to the walls become more so at higher wavenumbers, and at lower wavenumbers disappear entirely leaving just one vortex per (more rectangular) cell located close to the mid-plane of the channel. The disturbance quantities all vary relatively slowly over the domain, and are easily resolved.

The least-stable eigenmodes for the isothermal Maxwell Poiseuille (creeping) flow below about $k = 3$ are odd and correspond to plain, rectangular recirculation cells with a single vortex near the center of each cell. The least-stable modes above about $k = 3$, however, are even, and the streamline pattern for $\sigma = -.112 - .0993i$ at $k = 3.13$ is shown in Figure 24.

[Figure 24 about here.]

This even or sinuous mode is nearly stationary with a wave speed of 0.032, and is shown for the full channel width, as the secondary flow cells are no longer confined to a half-channel. The vortices move closer to the bounding walls with increasing wavenumber, and the polymeric stress (and configuration) pattern near the wall is very similar to that for the viscoelastic modes in Couette flow presented in Figure 17. As discussed earlier, these boundary layers (especially those for the xx-component of configuration and stress) become increasingly intense, narrow, and hence difficult to resolve, as the vortices move closer to the walls with increasing wavenumber.

5 Discussion

The stability calculations presented herein show that inertialess viscoelastic plane Couette and Poiseuille flows are stable to two-dimensional infinitesimal disturbances even when subject to relatively strong viscous dissipation ($Na \gg 1$); thermally induced gradients in the local viscosity and elasticity are insufficiently steep to drive an instability. At low and moderate wavenumbers, viscous heating destabilizes/stabilizes the least-stable energy modes for Couette/Poiseuille flow, while at high wavenumber it stabilizes the dominant viscoelastic modes. Decreasing the Peclet number, the polymeric viscosity ratio $(1 - \beta)$, or the polymer extensibility, appears to have a stabilizing effect. For isothermal creeping Poiseuille flow using the upper-convected Maxwell model, our calculations indicate that the least-stable mode is odd with a wavenumber based on channel half-width of $k = 1.5$.

In the absence of other driving mechanisms for elastic instability, there is insufficient coupling between the energy and viscoelastic modes to lead to growth of infinitesimal disturbances. This appears to be consistent with recent isothermal stability calculations by Wilson and Rallison (1999) that indicate very large transverse gradients in material properties are required to result in an instability. Although increased viscous heating effects do lead to transverse gradients in fluid elasticity and viscosity, as the Nahme number is increased, the magnitudes of the polymeric stresses decrease and thus eliminate onset of instability. Very recent computations by Sureshkumar and coworkers show that this balance can, however, change in flows with curvilinear streamlines (such as the Taylor-Couette geometry) which can exhibit purely elastic instability under isothermal conditions. Incorporating viscous heating effects can change both the critical onset conditions and the spatio-temporal characteristics of the resulting disturbance (Al-Mubaiyedh *et al.* 1999).

[Figure 25 about here.]

Exploratory computations at finite Reynolds numbers suggest that any instabilities in nonisothermal viscoelastic flows with rectilinear streamlines are due primarily to inertial effects. In Figure 25, we show the variation of $\mathrm{Re}(\sigma_{max})$ versus wavenumber k for Poiseuille flow at $Re = 100$ and $Re = 10^3$ for the case $Pe = 10^3$, $Na = 5$, $De = 5$, $\alpha = 60$, $\beta = 0.5$, and $b = \infty$. The stable curve for $Re = 100$ is visibly indistinguishable from the corresponding curve for $Re = 0$ on the scale of Figure 25, and hence it appears that a relatively large amount of inertia must be present in order to destabilize the flow. Our findings are the first to conclusively show that low-Reynolds-number polymeric melt extrudate instabilities such as sharkskin and melt fracture are probably not due to frictional dissipation alone, though thermal effects may still contribute to current theories involving polymer disentanglement or loss of adhesion near the wall (*e.g.* Barone *et al.* 1998, DeKee and Wissbrun 1998, Denn 1990, and references therein).

6 References

1. Al-Mubaiyedh U.A., Sureshkumar R., and Khomami B., Influence of the energetics on the stability of viscoelastic Taylor-Couette flow. *Phys. Fluids* **11**, 3217-3226 (1999).

2. Barone J.R., Plucktaveesak N., and Wang S.Q., Interfacial molecular instability mechanism for sharkskin phenomenon in capillary extrusion of linear polyethylenes. *J. Rheol.* **42**, 813-832 (1998).

3. Bird R.B., Armstrong R.C., and Hassager O., *Dynamics of Polymeric Liquids I.* Second Edition, John Wiley & Sons (1987a).

4. Bird R.B., Curtiss C.F., Armstrong R.C., and Hassager O., *Dynamics of Polymeric Liquids II.* Second Edition, John Wiley & Sons (1987b).

5. Davis S.H., Kriegsmann G.A., Laurence R.L., and Rosenblat S., Multiple solutions and hysteresis in steady parallel viscous flows. *Phys. Fluids* **26**, 1177-1181 (1983).

6. De Kee D., and Wissbrun K.F., Polymer Rheology. *Physics Today* **51**, 24-29 (1998).

7. Denn M.M., Issues in viscoelastic fluid mechanics. *Annu. Rev. Fluid Mech.* **22**, 13-34 (1990).

8. Drazin P.G., and Reid W.H., *Hydrodynamic Stability.* Cambridge University Press (1982).

9. Fornberg B., *A practical guide to pseudospectral methods.* Cambridge University Press (1995).

10. Gavis J., and Laurence R.L., Viscous heating in plane and circular flow between moving surfaces. *I&EC Fundamentals* **7**, 232-237 (1968).

11. Gorodtsov V.A., and Leonov A.I., On a linear instability of a plane parallel Couette flow of viscoelastic fluid. *J. Appl. Math. Mech.* **31**, 310-319 (1967).

12. Graham M.D., Effect of axial flow on viscoelastic Taylor-Couette instability. *J. Fluid Mech.* **360**, 341-374 (1998).

13. Gruntfest I.J., Thermal feedback in liquid flow; plane shear at constant stress. *Trans. Soc. Rheol.* **7**, 195-207 (1963).

14. Hatzikiriakos S.G., Kazatchkov I.B., and Vlassopoulos D., Interfacial phenomena in the capillary extrusion of metallocene polyethylenes. *J. Rheol.* **41**, 1299-1316 (1997).

15. Ho T.C., Denn M.M., and Anshus B.E., Stability of low Reynolds number flow with viscous heating. *Rheol. Acta* **16**, 61-68 (1977).

16. Johns L.E., and Narayanan R., Frictional heating in plane Couette flow. *Proc. R. Soc. Lond.* A **453**, 1653-1670 (1997).

17. Joseph D.D., Variable viscosity effects on the flow and stability of flow in channels and pipes. *Phys. Fluids* **7**, 1761-1771 (1964).

18. Joseph D.D., Stability of frictionally-heated flow. *Phys. Fluids* **8**, 2195-2200 (1965).

19. Khayat R.E., Nonlinear overstability in the thermal convection of viscoelastic fluids. *J. Non-Newt. Fluid Mech.* **58**, 331-356 (1995).

20. Kolodner P., Oscillatory convection in viscoelastic DNA suspensions. *J. Non-Newt. Fluid Mech.* **75**, 167-192 (1998).

21. Larson R.G., Instabilities in viscoelastic flows. *Rheol. Acta* **31**, 213-263 (1992).

22. Lee K.-C., and Finlayson B.A., Stability of plane Poiseuille and Couette flow of a Maxwell fluid. *J. Non-Newt. Fluid Mech.* **21**, 65-78 (1986).

23. Marrucci G., The free energy constitutive equation for polymer solutions from the dumbbell model. *Trans. Soc. Rheol.* **16**, 321-330 (1972).

24. Orszag S.A., Accurate solution of the Orr-Sommerfeld stability equation. *J. Fluid Mech.* **50**, 689-703 (1971).

25. Pearson J.R.A., *Mechanics of Polymer Processing*, Elsevier, London (1985).

26. Peters G.W.M., and Baaijens P.T., Modelling of non-isothermal viscoelastic flows. *J. Non-Newt. Fluid Mech.* **68**, 205-224 (1997).

27. Petrie C.J.S., and Denn M.M., Instabilities in Polymer Processing. *AIChE J.* **22**, 209-236 (1976).

28. Porteous K.C., and Denn M.M., Linear stability of plane Poiseuille flow of viscoelastic liquids. *Trans. Soc. Rheol.* **16**, 295-308 (1972).

29. Porteous K.C., and Denn M.M., Nonlinear stability of plane Poiseuille flow of viscoelastic liquids. *Trans. Soc. Rheol.* **16**, 309-319 (1972).

30. Renardy M., and Renardy Y., Linear stability of plane Couette flow of an upper convected Maxwell fluid. *J. Non-Newt. Fluid Mech.* **22**, 23-33 (1986).

31. Shah Y.T., and Pearson J.R.A., Stability of non-isothermal flow in channels - I. Temperature-dependent Newtonian fluid without heat generation. *Chem. Eng. Sci.* **28**, 2079-2088 (1974a).

32. Shah Y.T., and Pearson J.R.A., Stability of non-isothermal flow in channels - II. Temperature-dependent power-law fluids without heat generation. *Chem. Eng. Sci.* **29**, 737-746 (1974b).

33. Shah Y.T., and Pearson J.R.A., Stability of non-isothermal flow in channels - III. Temperature-dependent power-law fluids with heat generation. *Chem. Eng. Sci.* **29**, 1485-1493 (1974c).

34. Skul'skiy O.I., Slavnov Y.V., and Shakirov N.V., The hysteresis phenomenon in non-isothermal channel flow of a Non-Newtonian liquid. *J. Non-Newt. Fluid Mech.* **81**, 17-26 (1999).

35. Su Y.-Y., and Khomami B., Interfacial stability of multilayer viscoelastic fluids in slit and converging channel die geometries. *J. Rheol.* **36**, 357-387 (1992).

36. Sukanek P.C., Goldstein C.A., and Laurence R.L., The stability of plane Couette flow with viscous heating. *J. Fluid Mech.* **57**, 651-670 (1973).

37. Sureshkumar R., and Beris A.N., Linear stability analysis of viscoelastic Poiseuille flow using an Arnoldi-based orthogonalization algorithm. *J. Non-Newt. Fluid Mech.* **56**, 151-182 (1995).

38. Wiest J.M., Non-equilibrium energetic effects in the inception of shear flow of dilute polymer solutions. *Chem. Eng. Sci.* **51**, 1441-1449 (1996).

39. Wilson H.J., and Rallison J.M., Short wave instability of co-extruded elastic liquids with matched viscosities. *J. Non-Newt. Fluid Mech.* **72**, 237-251 (1997).

40. Wilson H.J., and Rallison J.M., Instability of channel flows of elastic liquids having continuously stratified properties. *J. Non-Newt. Fluid Mech.* **85**, 273-298 (1999).

41. Wilson H.J., Renardy M., and Renardy Y., Structure of the spectrum in zero Reynolds number shear flow of the UCM and Oldroyd-B liquids. *J. Non-Newt. Fluid Mech.* **80**, 251-268 (1998).

42. Winter H.H., Viscous dissipation in shear flows of molten polymers. *Adv. Heat Transfer* **13**, 205-267 (1977).

43. Yueh C.-S., and Weng C.-I., Linear stability analysis of plane Couette flow with viscous heating. *Phys. Fluids* **8**, 1802-1813 (1996).

44. Zebib A., Removal of spurious modes encountered in solving stability problems by spectral methods. *J. Comp. Phys.* **70**, 521-525 (1987).

List of Figures

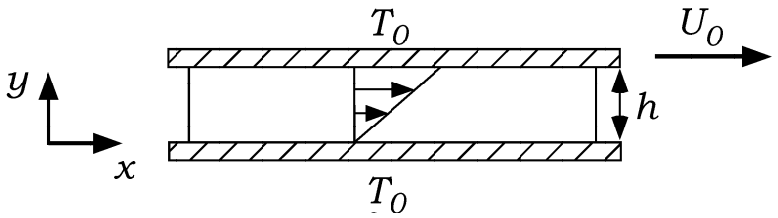

(a)

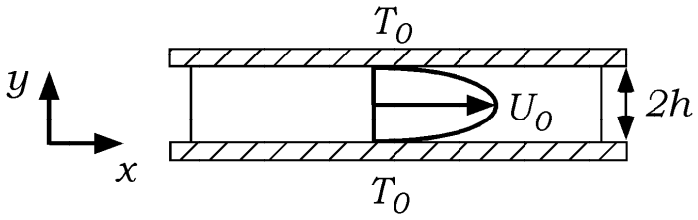

(b)

Figure 1: (a) Definition diagram for plane Couette flow. The bottom plate is stationary while the top plate translates at a constant velocity U_0. Both plates are maintained at a constant temperature T_0, and are separated by a distance h. (b) Definition diagram for plane Poiseuille flow. The top and bottom plates are stationary. A constant-average negative pressure gradient in the x-direction causes a flow with centerline velocity U_0. Both plates are maintained at a constant temperature T_0, and are separated by a distance $2h$.

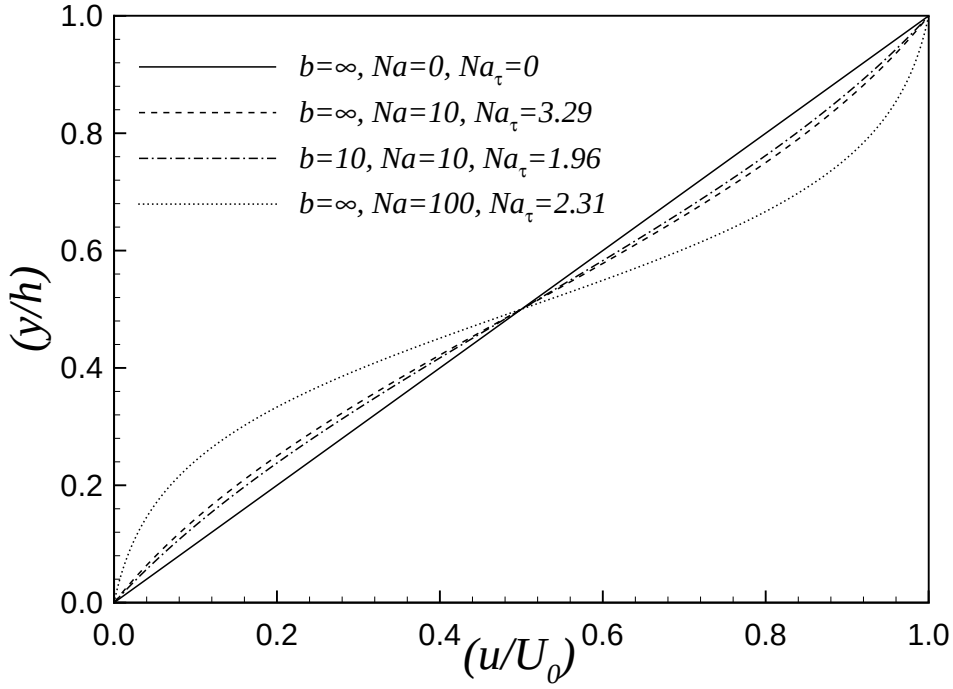

Figure 2: Couette base flow velocity profiles for $b = \infty$ with $Na = 0$, 10, and 100, as well as for $b = 10$ with $Na = 10$, $De = 10$, $\alpha = 60$, and $\beta = 0.5$.

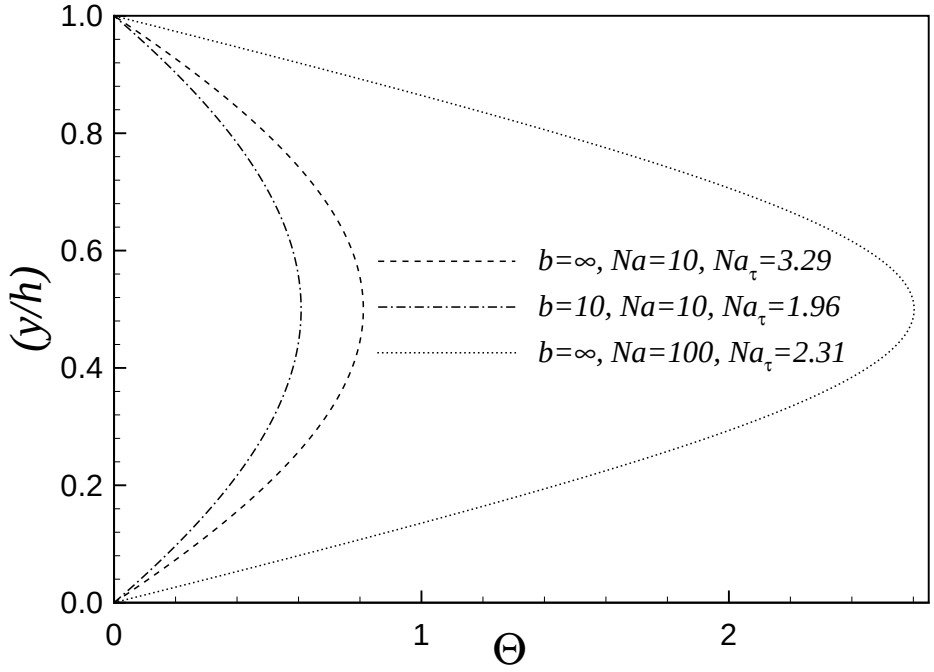

Figure 3: Couette base flow temperature profiles for $b = \infty$ with $Na = 10$ and 100, as well as for $b = 10$ with $Na = 10$, $De = 10$, $\alpha = 60$, and $\beta = 0.5$.

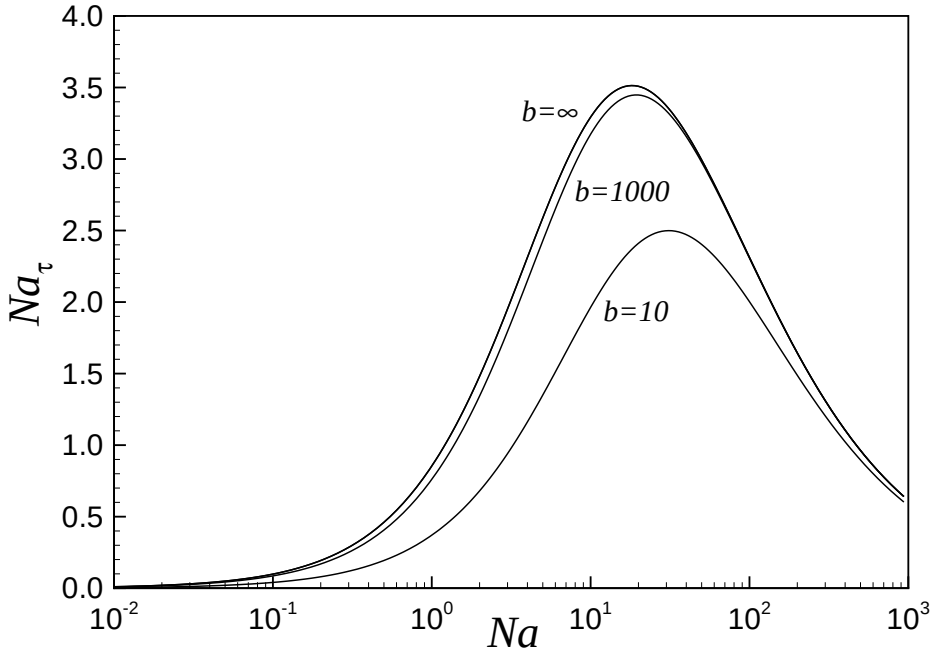

(a)

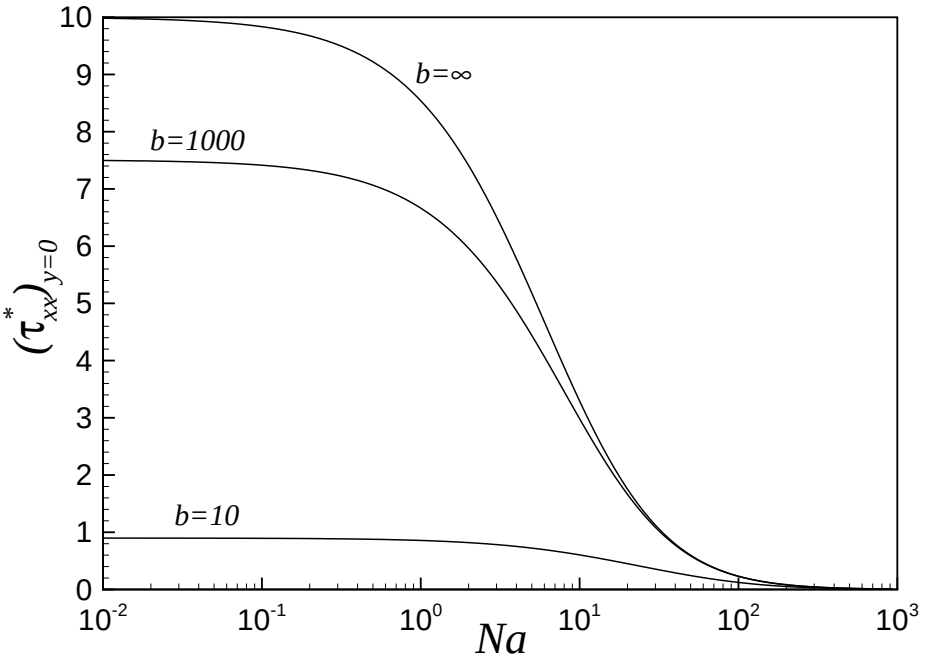

(b)

Figure 4: (a) Couette flow constitutive plot of Na_τ versus Na for $b = 10$, 1000, and ∞, with $De = 10$, $\alpha = 60$, and $\beta = 0.5$. (b) As (a) but for normal stress at the wall versus Na.

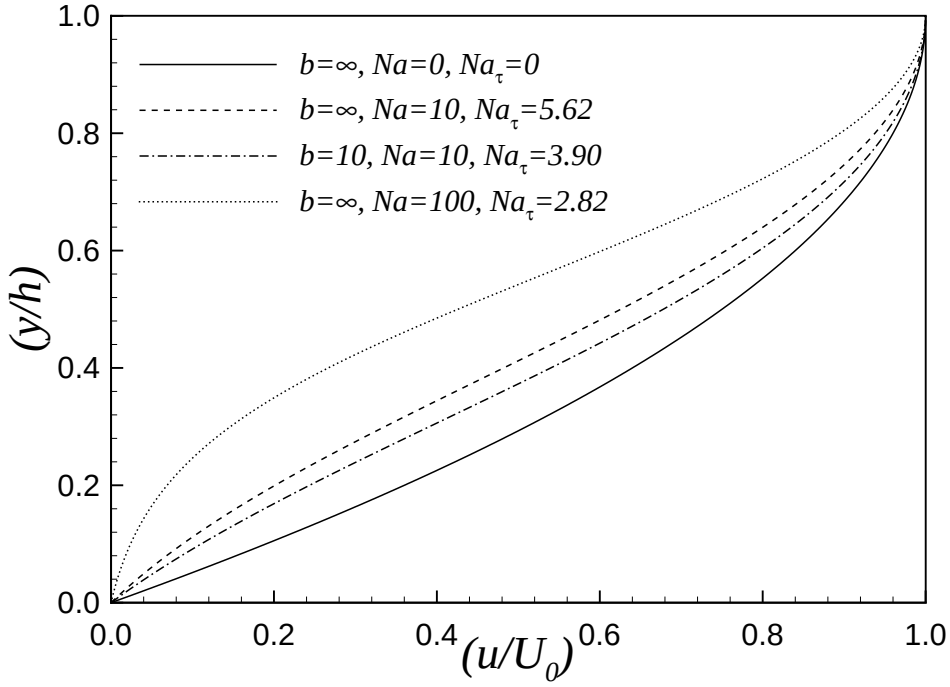

Figure 5: Poiseuille base flow velocity profiles for $b = \infty$ with $Na = 0$, 10, and 100, as well as for $b = 10$ with $Na = 10$, $De = 10$, $\alpha = 60$, and $\beta = 0.5$.

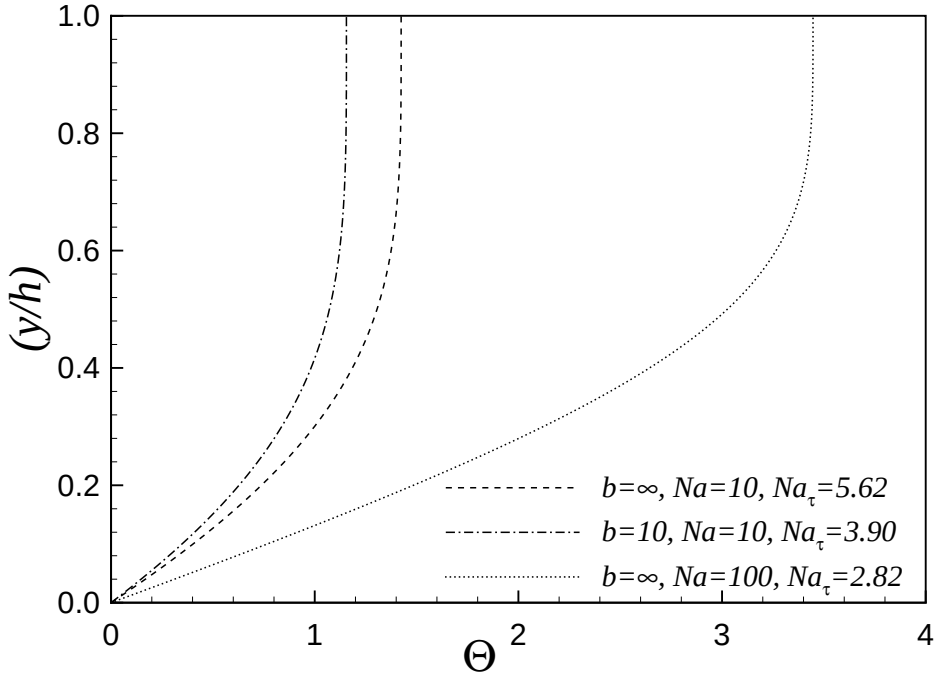

Figure 6: Poiseuille base flow temperature profiles for $b = \infty$ with $Na = 10$ and 100, as well as for $b = 10$ with $Na = 10$, $De = 10$, $\alpha = 60$, and $\beta = 0.5$.

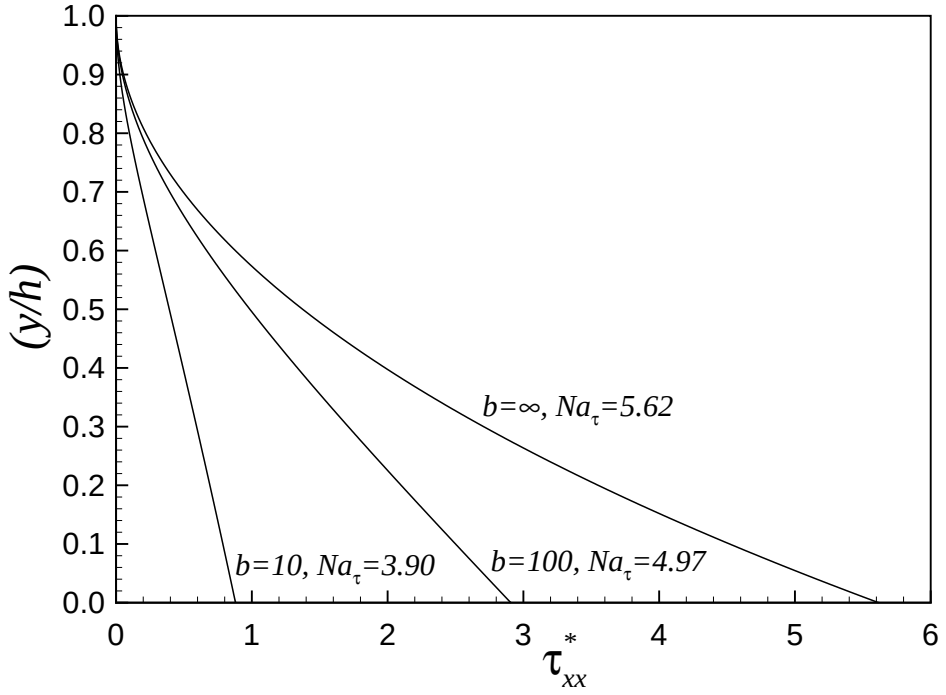

Figure 7: Poiseuille base flow normal stress profiles comparing $b = 10$, 100, and ∞, for $Na = 10$, $De = 10$, $\alpha = 60$, and $\beta = 0.5$.

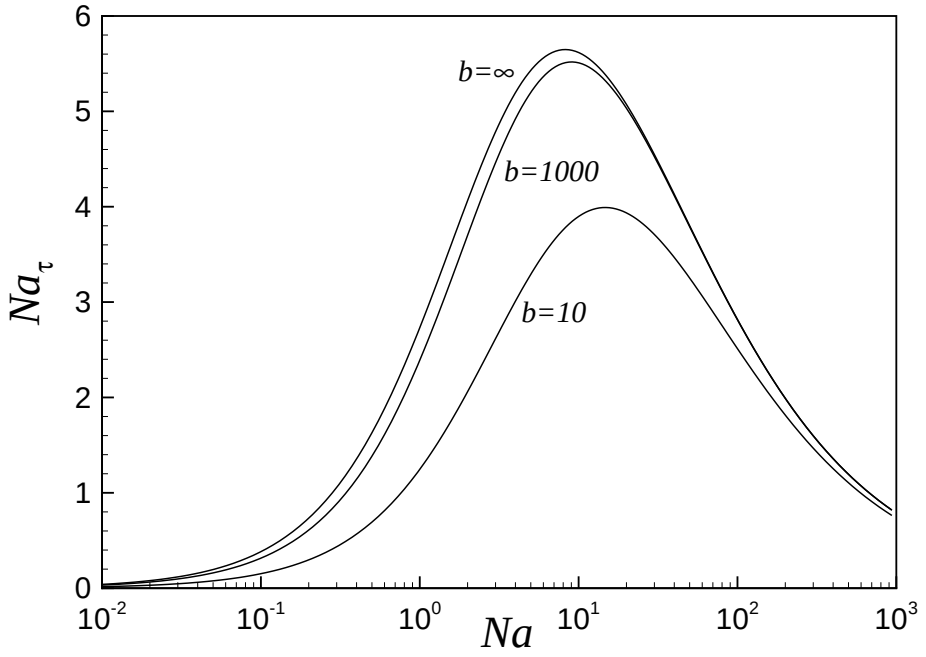

(a)

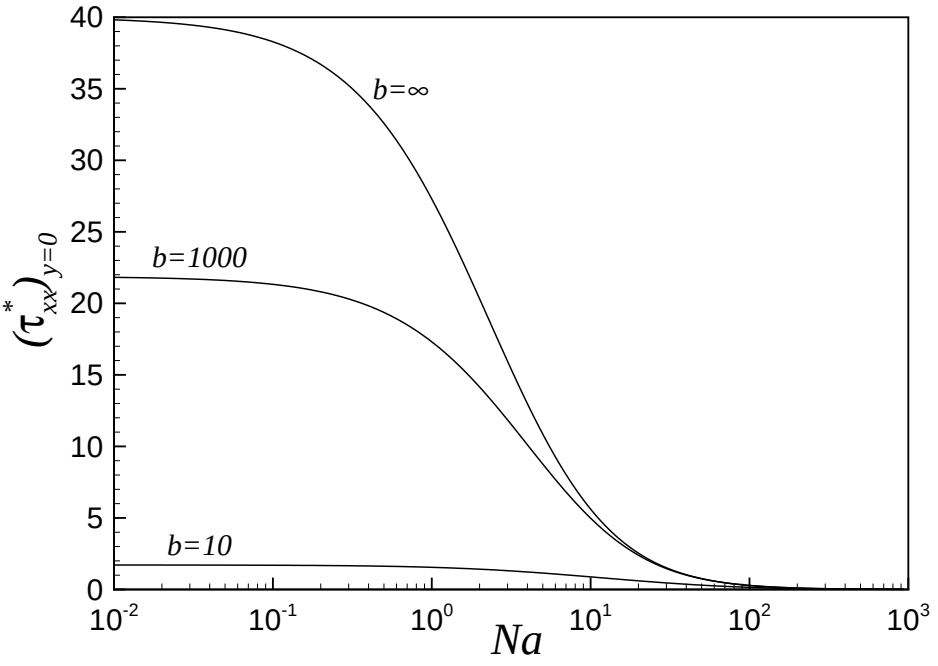

(b)

Figure 8: (a) Poiseuille flow constitutive plot of Na_τ versus Na for $b = 10$, 1000, and ∞, with $De = 10$, $\alpha = 60$, and $\beta = 0.5$. (b) As (a) but for normal stress at the wall versus Na.

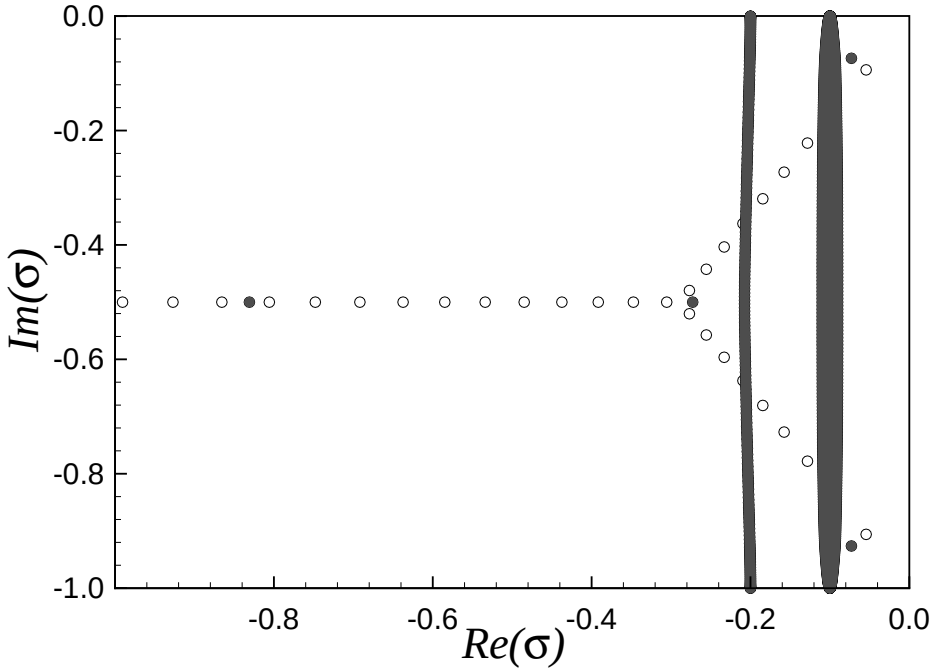

(a)

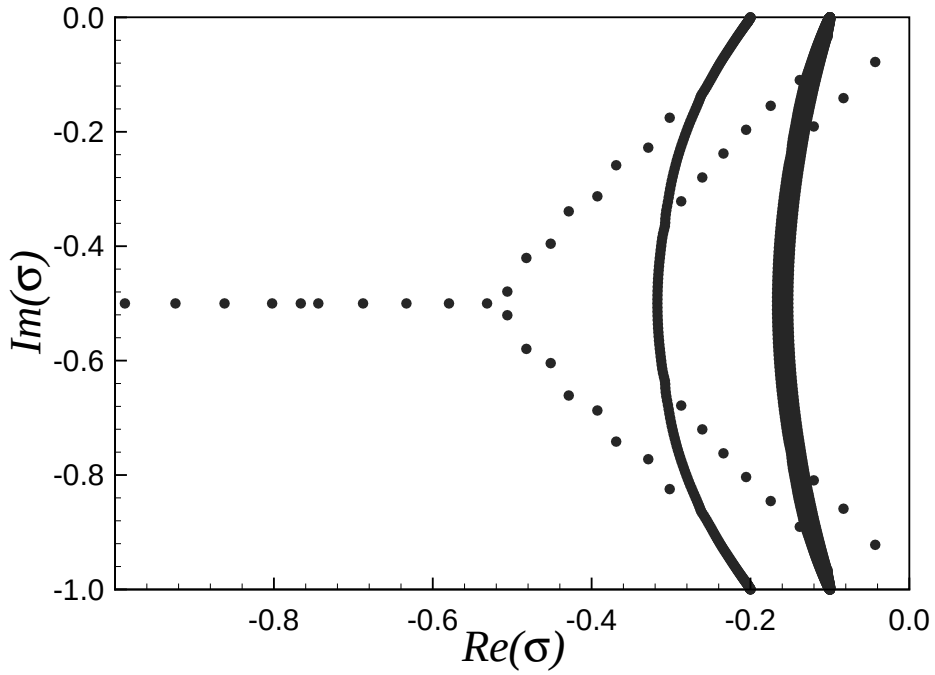

(b)

Figure 9: (a) Couette flow eigenvalue spectrum for $k = 1$, $Pe = 10^4$, $Na = 0$, $De = 10$, $\alpha = 60$, $\beta = 0.5$, $b = \infty$, and $N = 250$. The solid circles correspond to the eigenvalues of the isothermal stability problem, while the hollow circles correspond to those of the energy equation (25). (b) As (a) but for $Na = 5$.

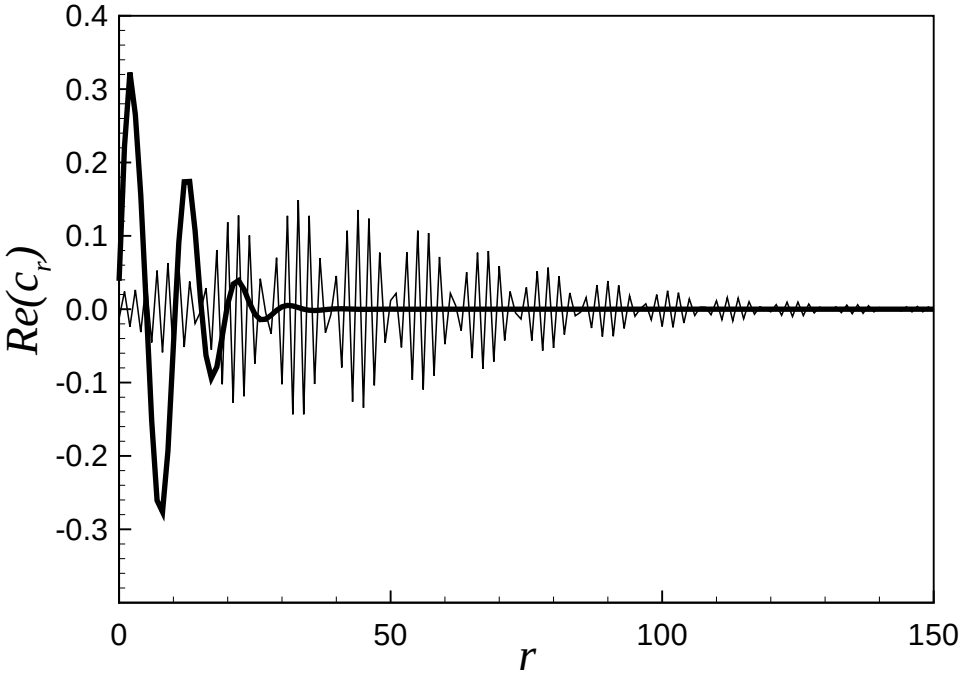

Figure 10: Convergence of a_{xx}-series coefficient c_r with number of terms r for the least-stable (discrete) Couette flow eigenmodes at wavenumbers $k = 1$ (thick line) and $k = 5$ (thin line), where $Pe = 10^4$, $Na = 5$, $De = 10$, $\alpha = 60$, $\beta = 0.5$, and $b = \infty$.

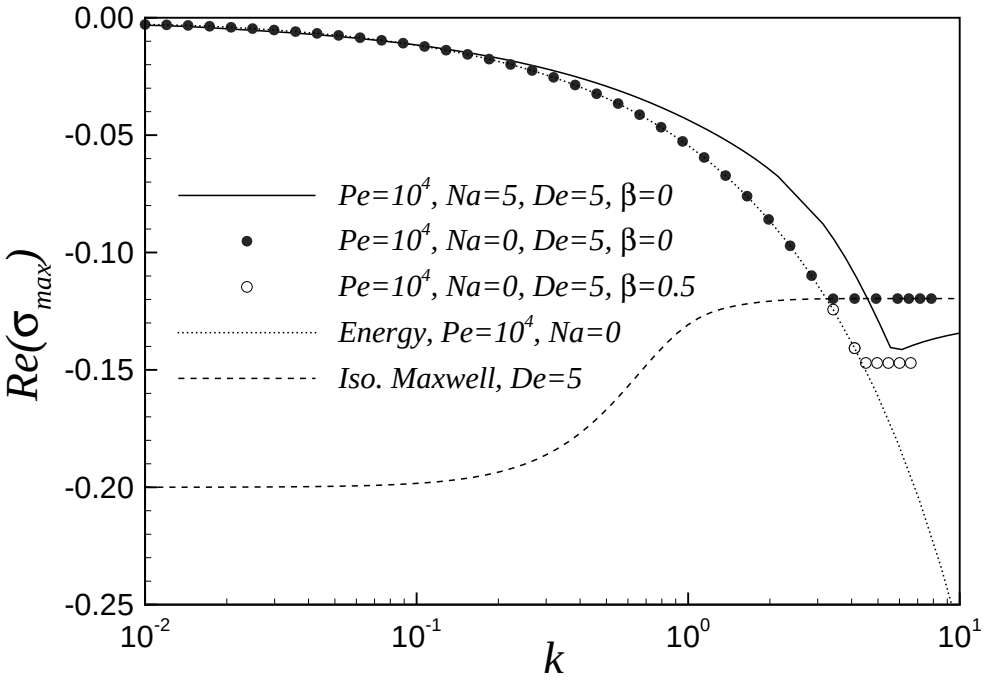

Figure 11: Temporal part of least-stable Couette flow eigenvalue, $\mathrm{Re}(\sigma_{max})$, versus k for $Re = 0$, $\alpha = 60$, $b = \infty$, at $De = 5$, with comparison to known isothermal results.

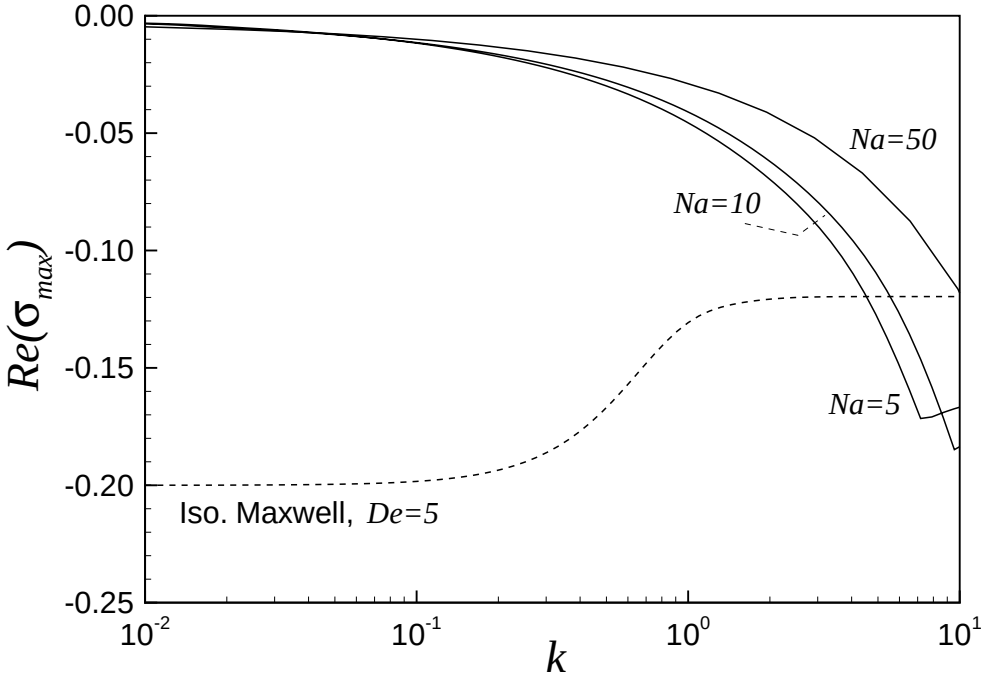

Figure 12: Temporal part of least-stable Couette flow eigenvalue, $\mathrm{Re}(\sigma_{max})$, versus k for $Na = 5$, 10, and 50 with $Re = 0$, $Pe = 10^4$, $De = 5$, $\alpha = 60$, $\beta = 0.5$, and $b = \infty$.

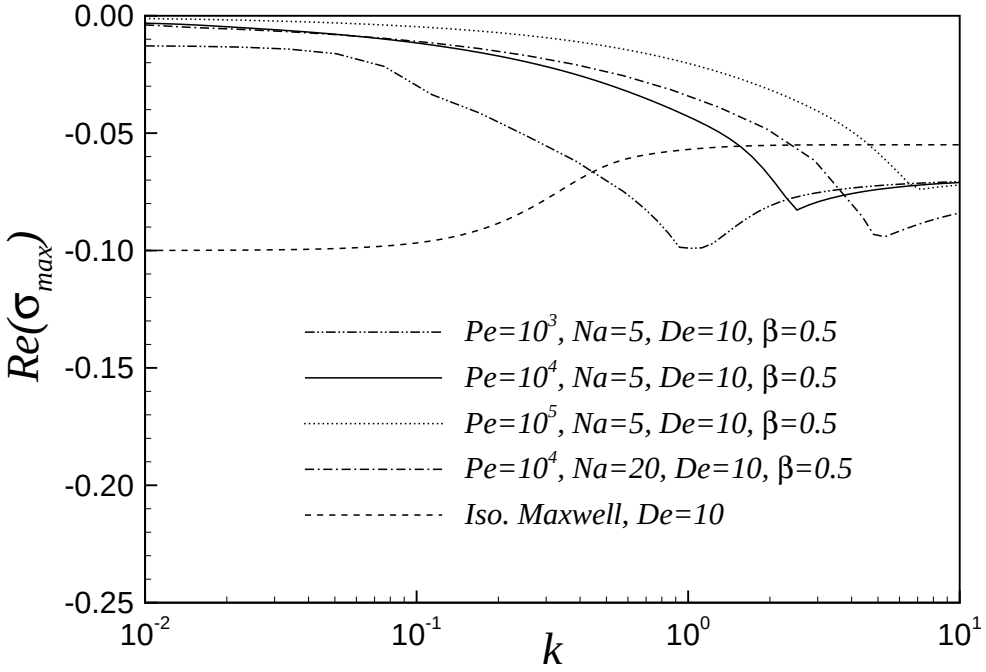

Figure 13: Temporal part of least-stable Couette flow eigenvalue, $\mathrm{Re}(\sigma_{max})$, versus k for $Pe = 10^3$, 10^4, and 10^5 at $De = 10$ with $Re = 0$, $\alpha = 60$, and $b = \infty$.

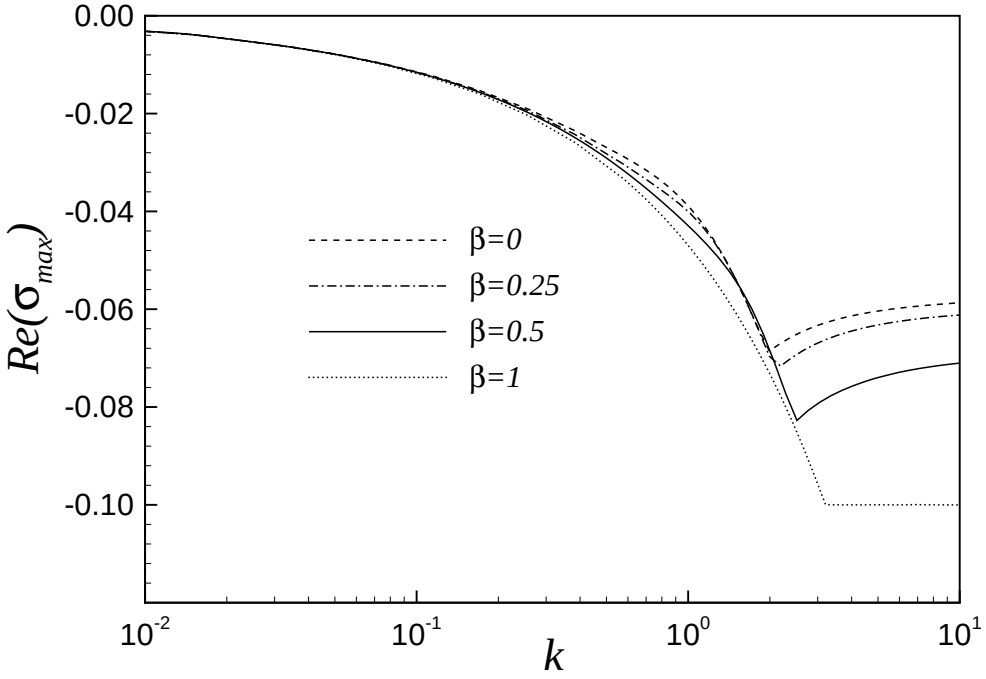

Figure 14: Temporal part of least-stable Couette flow eigenvalue, $\mathrm{Re}(\sigma_{max})$, versus k for different values of β at $Re = 0$, $Pe = 10^4$, $Na = 5$, $De = 10$, $\alpha = 60$, and $b = \infty$.

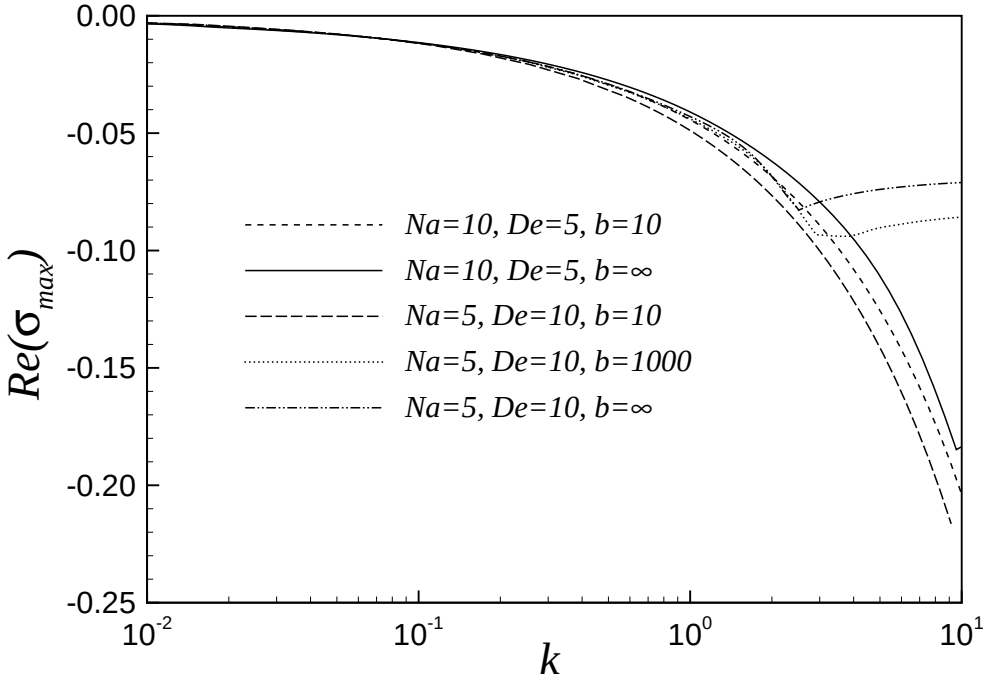

Figure 15: Temporal part of least-stable Couette flow eigenvalue, $\mathrm{Re}(\sigma_{max})$, versus k for different values of b at $Re = 0$, $Pe = 10^4$, $\alpha = 60$, and $\beta = 0.5$.

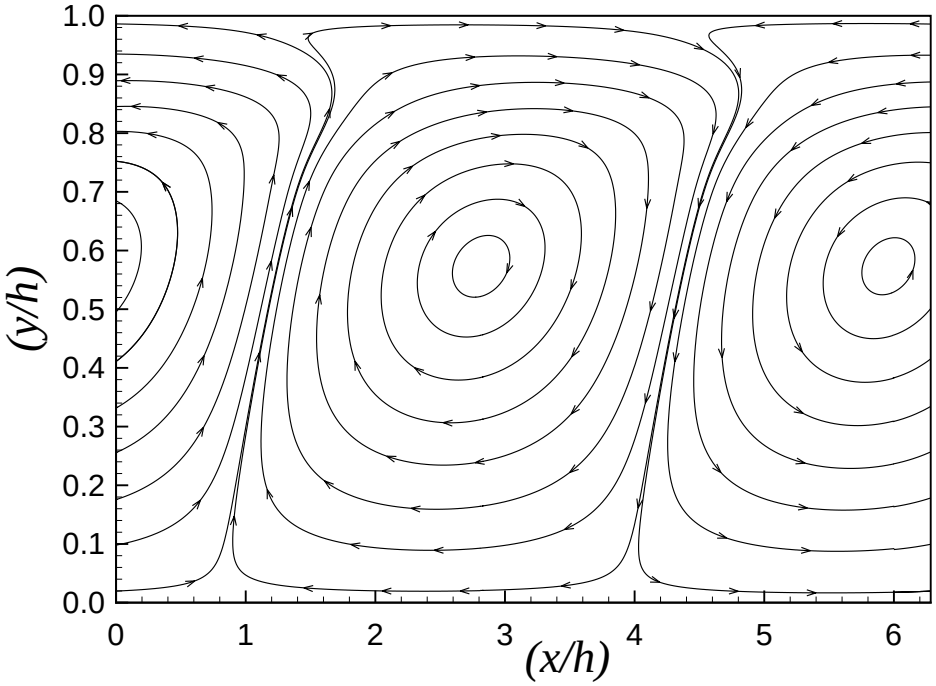

Figure 16: Couette flow perturbation streamlines for $\sigma = -0.043 - 0.992i$ at $k = 1$ with $Pe = 10^4$, $Na = 5$, $De = 10$, $\alpha = 60$, $\beta = 0.5$, and $b = \infty$.

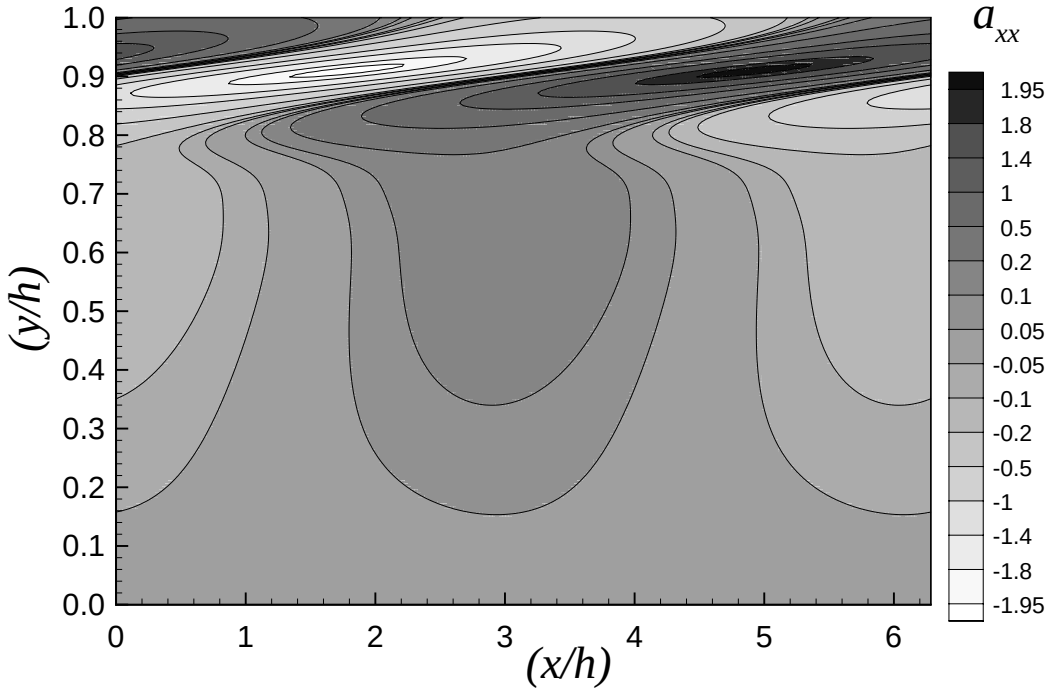

Figure 17: Couette flow contour plot of a_{xx} for $\sigma = -0.043 - 0.992i$ at $k = 1$ with $Pe = 10^4$, $Na = 5$, $De = 10$, $\alpha = 60$, $\beta = 0.5$, and $b = \infty$.

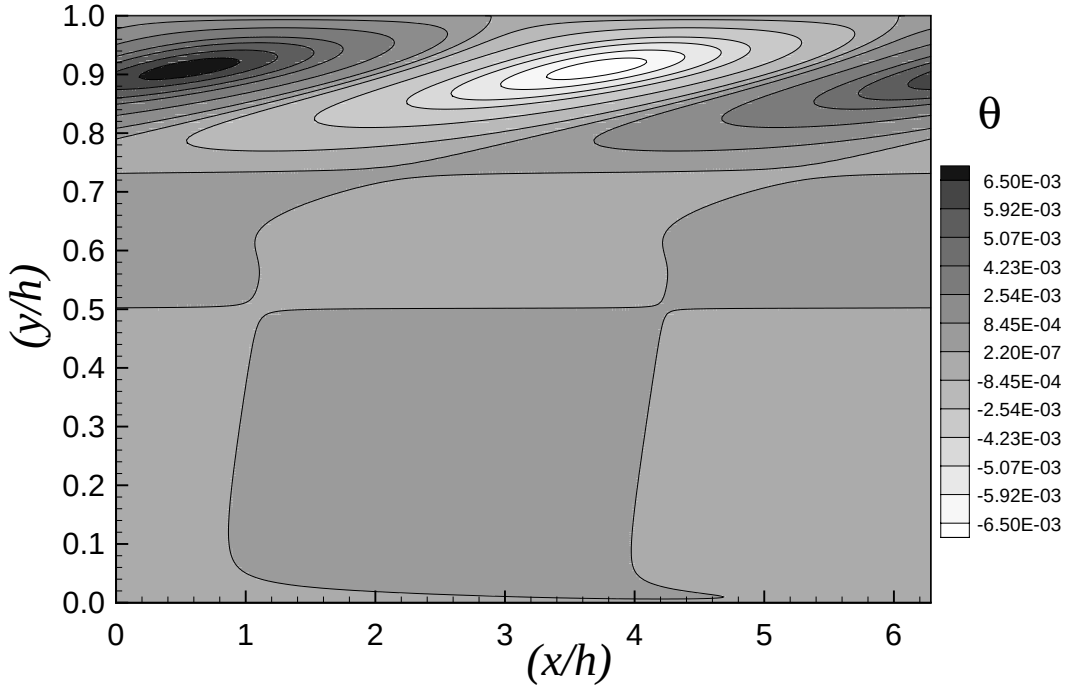

Figure 18: Couette flow contour plot of θ for $\sigma = -0.043 - 0.992i$ at $k = 1$ with $Pe = 10^4$, $Na = 5$, $De = 10$, $\alpha = 60$, $\beta = 0.5$, and $b = \infty$.

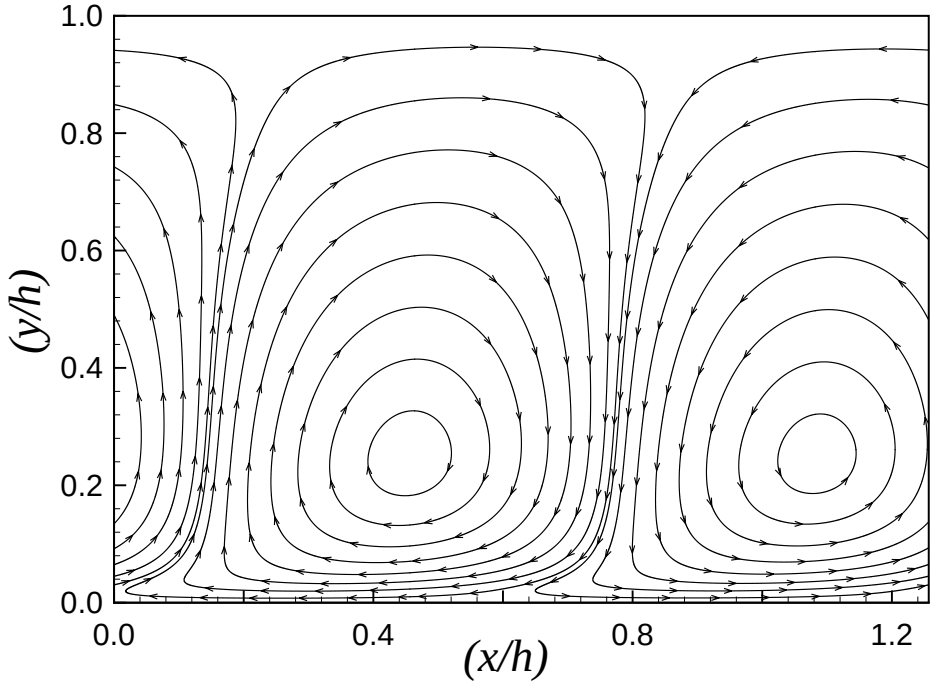

Figure 19: Couette flow perturbation streamlines for $\sigma = -0.074 - 0.067i$ at $k = 5$ with $Pe = 10^4$, $Na = 5$, $De = 10$, $\alpha = 60$, $\beta = 0.5$, and $b = \infty$.

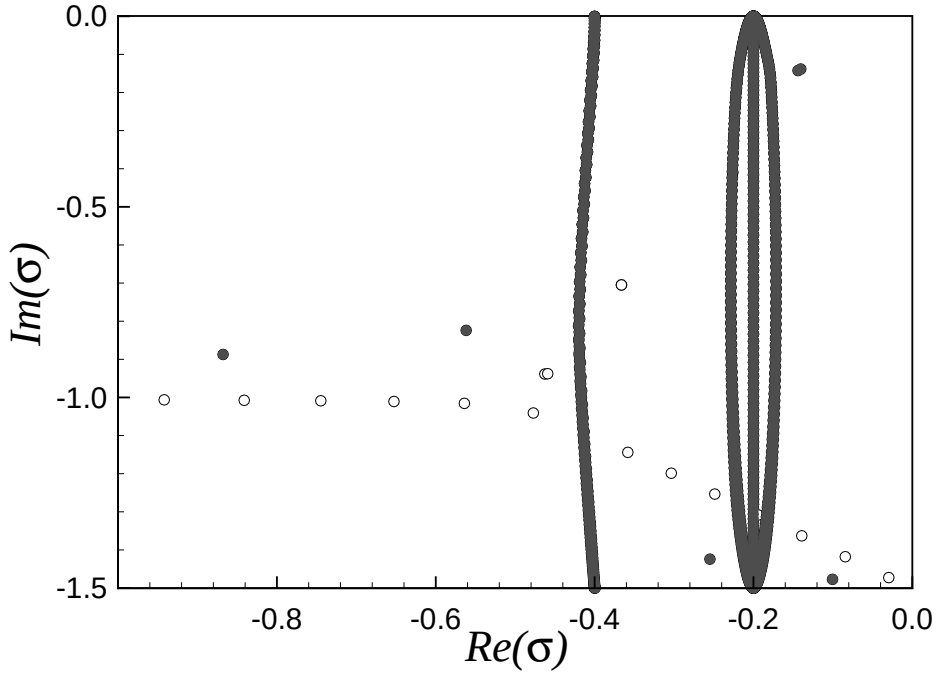

(a)

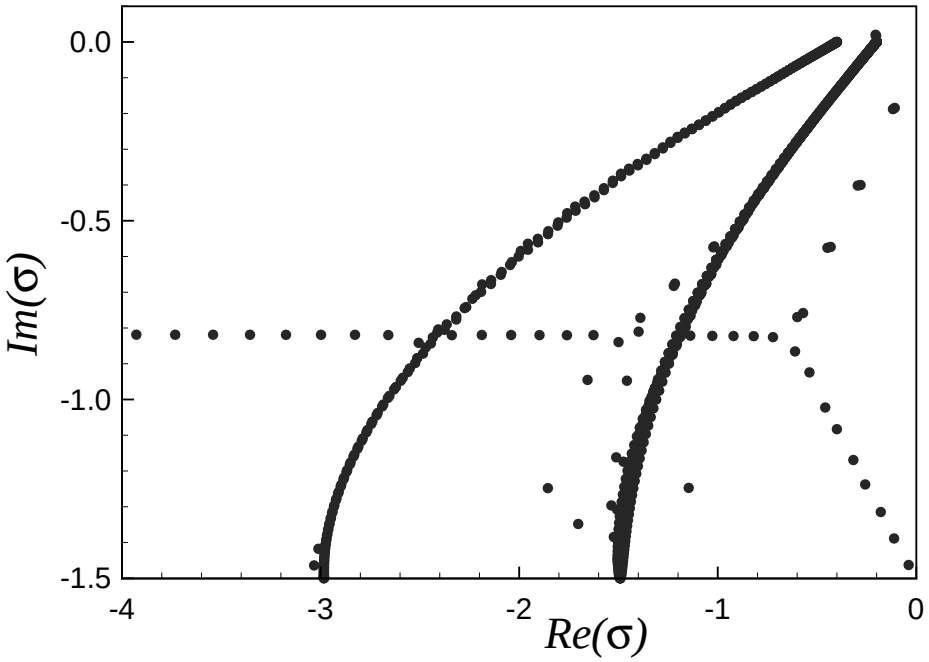

(b)

Figure 20: (a) Poiseuille flow eigenvalue spectrum for $k = 1.5$, $Pe = 10^3$, $Na = 0$, $De = 5$, $\alpha = 60$, $\beta = 0.5$, $b = \infty$, and $N = 250$. The solid circles correspond to the eigenvalues of the isothermal stability problem, while the hollow circles correspond to those of the energy equation at zero Nahme number. (b) As (a) but for $Na = 20$.

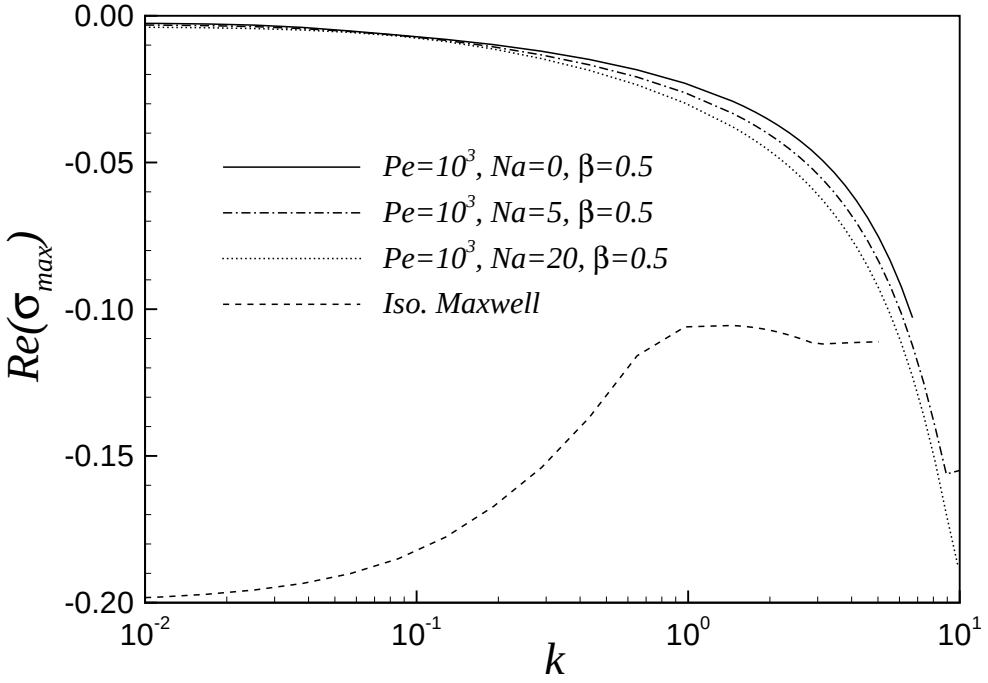

Figure 21: Temporal part of least-stable Poiseuille flow eigenvalue, $\mathrm{Re}(\sigma_{max})$, versus k for $Re = 0$, $\alpha = 60$, $b = \infty$, at $De = 5$, with comparison to isothermal results.

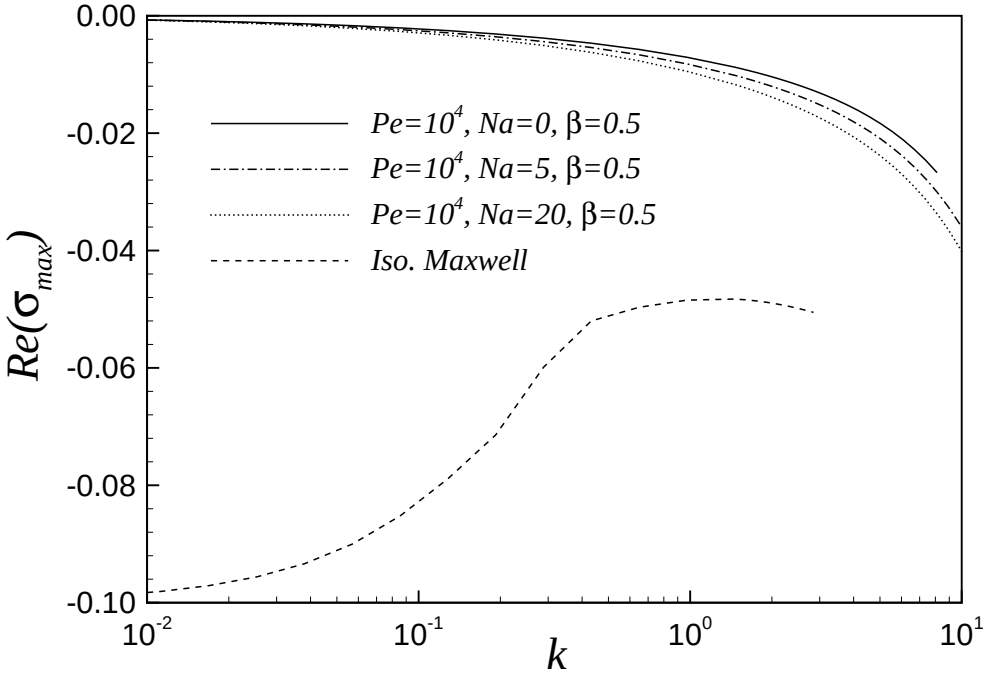

Figure 22: Temporal part of least-stable Poiseuille flow eigenvalue, $\mathrm{Re}(\sigma_{max})$, versus k for $Re = 0$, $\alpha = 60$, $b = \infty$, at $De = 10$, with comparison to isothermal results.

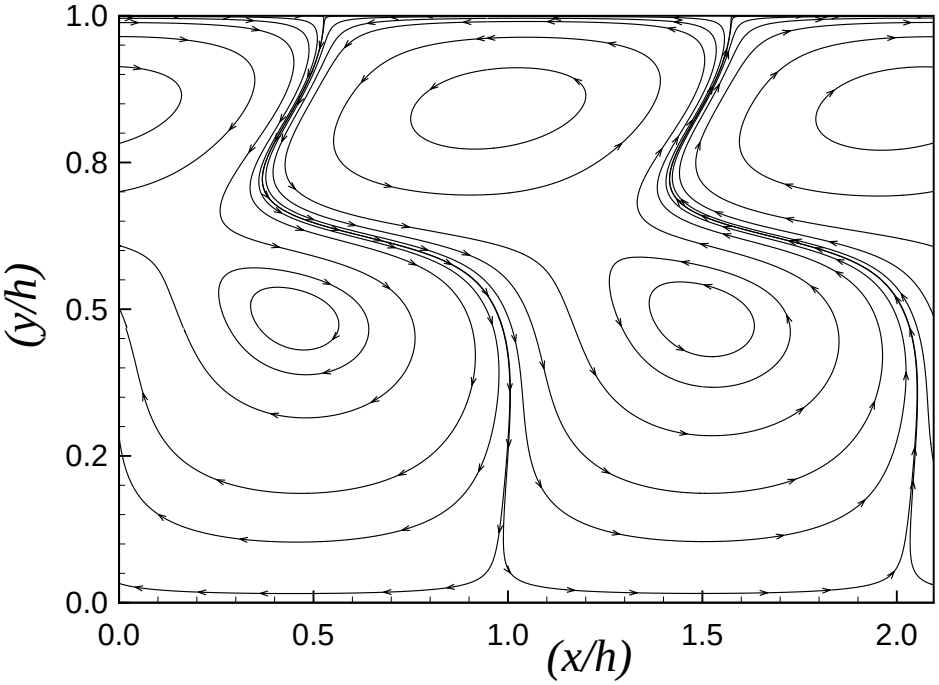

Figure 23: Poiseuille flow perturbation streamlines for $\sigma = -0.061 - 2.95i$ at $k = 3$ with $Pe = 10^3$, $Na = 20$, $De = 5$, $\alpha = 60$, $\beta = 0.5$, and $b = \infty$.

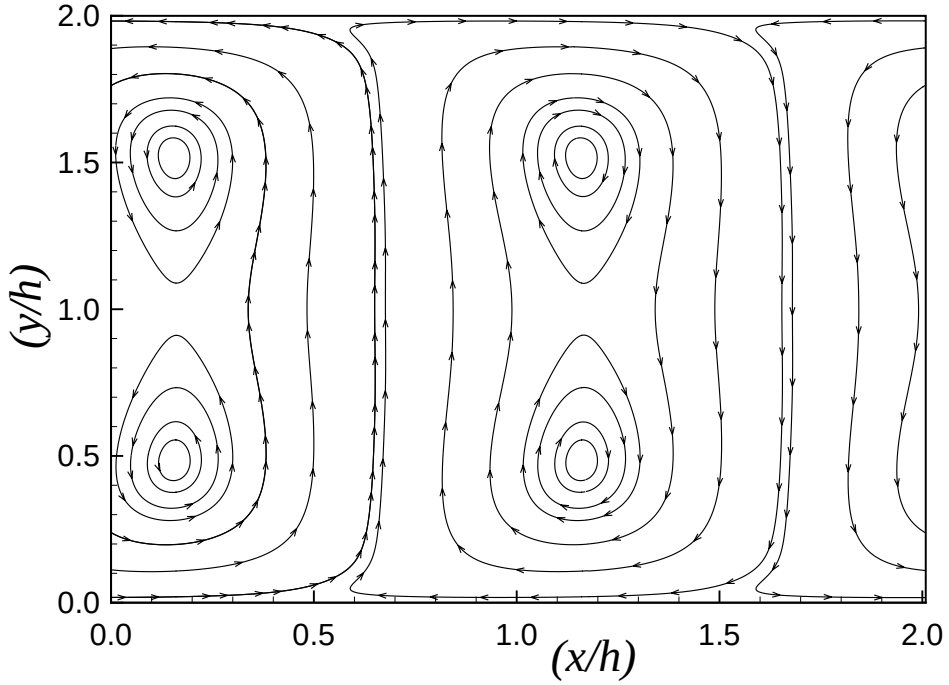

Figure 24: Poiseuille flow perturbation streamlines for $\sigma = -.112 - .0993i$ at $k = 3.13$ with isothermal Maxwell model at $De = 5$.

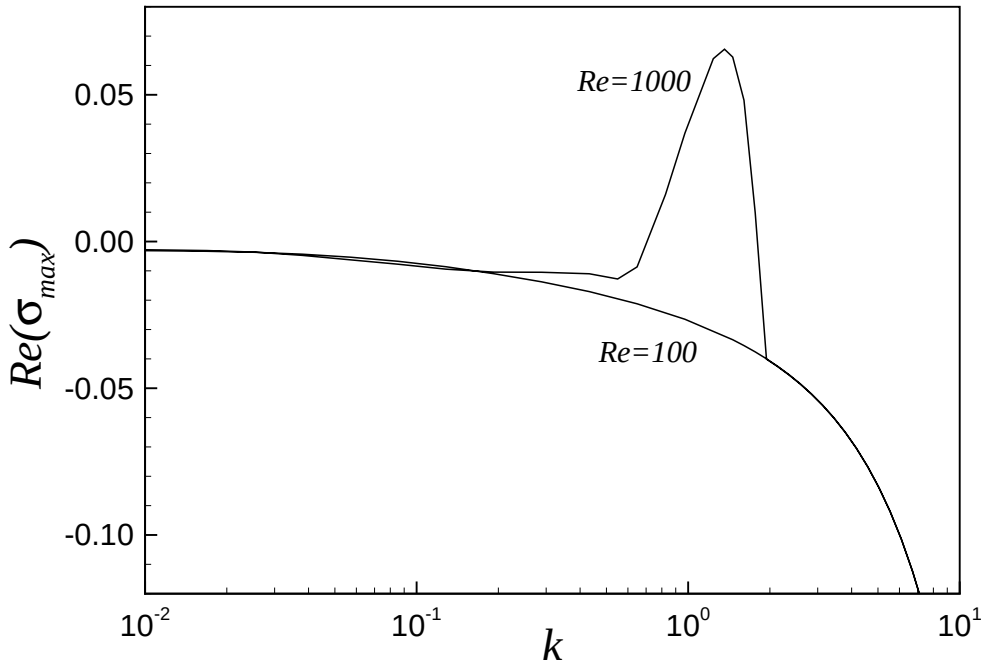

Figure 25: Temporal part of least-stable Poiseuille flow eigenvalue, $\mathrm{Re}(\sigma_{max})$, versus k for $Re = 100$ and 10^3 with $Pe = 10^3$, $Na = 5$, $De = 5$, $\alpha = 60$, $\beta = 0.5$, and $b = \infty$.